2009

Process-oriented modeling studies of the 5500-km-long boundary flow off western and southern Australia

Batteen, Mary L.

Process-oriented modeling studies of the 5500-km-long boundary flow off western and southern Australia

Mary L. Batteen *, Henry A. Miller

Department of Oceanography, Naval Postgraduate School, 833 Dyer Road, Room 328, Monterey, CA 93943-5193, USA

ARTICLE INFO

ABSTRACT

While the unique character of the coastal current system off the western and southern coasts of Australia has been recognized, this vast 5500-km-long boundary flow has been studied far less than other current systems of the world. Recent observational studies from satellite altimetry and climatology are consistent with a continuous current extending from its origin at the North West Cape to the southern tip of Tasmania. To date, coastal modeling studies have focused on either the western Australian coast to Esperance or on southern Australia. There has been no process-oriented modeling study of the entire region that would allow the systematic exploration of the two independent forcing mechanisms (i.e., wind-forcing and thermohaline gradients) and their interactions that have been noted to act in a synergistic manner to maintain the longest continuous coastal current system in the world.

This study uses a regional circulation model (in this case the Princeton Ocean Model (POM)) to systematically address the roles the forcing mechanisms play in generating and maintaining the major features of this continuous coastal current system. Several process-oriented experiments, arranged in order of increasing complexity, are explored. The results show that, even in the absence of bottom topography, a continuous 5500 km coastal current system can be generated by wind forcing or by thermohaline forcing. If wind forcing alone is used, coastal currents in the direction of the wind and opposing undercurrents can be generated. If thermohaline forcing alone is used, coastal currents in the opposite direction of the wind and subsurface currents similar to the Flinders Current can be generated.

The addition of topography shows that topography is responsible for the currents' shelf break locations and, for broad shelf regions, can separate the surface flow into two cores, one at the coast and one over the shelf. On the west coast, topographic beta due to the continental slope prevents currents from becoming broader and drifting offshore. The combination of wind forcing, thermohaline gradients and topography show that swift currents forced by thermohaline gradients are slowed to more realistic speeds by opposing wind and by topography. Meanders and eddies result from the opposition of surface and subsurface currents as well as from thermohaline and wind forcing. The results illustrate that the 5500-km-long current system over the shelf break can be maintained year-long due to the two independent forcing mechanisms, their interactions, and the strong trapping effect of bottom topography.

The seasonal and daily wind-forcing experiments highlight both the seasonal and interannual variability of this complex current system. The Leeuwin Current along the western coast is slightly stronger in winter (July) than summer (January). There is much greater mesoscale activity in January when the opposing winds are strongest. The results also show that, although upwelling has been observed only in the summer in the Capes Current region, upwelling occurs intermittently in the 2001 winter but not in the 2001 summer. This illustrates that, depending on the strength of the forcing mechanism, such as strong equatorward winter 2001 winds, features such as upwelling on the west coast, usually thought to exist in the summer but only intermittently, can occur in different seasons. Along the southern coast, a gyre forms intermittently in the Great Australian Bight in summer, but the flow is constantly eastward across the entire shelf in winter. The production of upwelling in the Great Australian Bight during the 2000 summer but not during the 2001 summer is an indication of the importance of interannual variability. Overall, the results of this process-oriented study compare well with available observations off western and southern Australia.

Published by Elsevier Ltd.

---

* Corresponding author. Tel.: +1 831 656 3265; fax: +1 831 656 2712.
  E-mail address: mlbattee@nps.edu (M.L. Battee).

1. Introduction

1.1. Observational background

Along a typical subtropical eastern ocean boundary, the prevailing winds are equatorward, or at least have a large equatorward component. These equatorward winds generate an offshore Ekman transport and cause upwelling near the coast. With cold upwelled water along the coast and warmer water offshore, the sea surface slopes down toward the coast, resulting in a geostrophically balanced equatorward current moving in the same direction as the wind. Since the surface slopes downward from the equator toward the pole in the alongshore direction, this surface current flows against a pressure gradient. This pressure gradient forces a poleward undercurrent at depths of 100–300 m (McCreary et al., 1986).

The circulation off the west coast of Australia, the eastern boundary of the Indian Ocean, is quite different from the other subtropical eastern boundary current systems even though the wind is equatorward year-round. There is no persistent upwelling, although there can be areas of seasonal equatorward surface flow favorable for upwelling such as the Ningaloo Current (Woo et al., 2006; Woo and Pattiartchi, 2008) and the Capes Current (Gersbach et al., 1999; Pearce and Pattiaratchi, 1999). The Leeuwin Current (LC) is narrow and flows poleward in opposition to the prevailing wind, and there is an equatorward undercurrent (see Fig. 1a for locations of the large-scale currents and undercurrents off the western and southern coasts of Australia). The sea surface slopes down toward the pole, so the current flows with the pressure gradient (Thompson, 1984; McCreary et al., 1986; Smith et al., 1991; Batteen and Butler, 1998).

There are other examples of surface currents which flow against the wind. The Davidson Current flows poleward off the coast of California when the equatorward winds relax in late fall and winter (Batteen et al., 2003). A poleward countercurrent also appears off the west coast of India in the winter (McCreary et al., 1986). However, the Leeuwin Current along the west coast of Australia is unique. First, the other examples are thought to be undercurrents which surface during a short season of the year when the equatorward winds relax. In contrast, the Leeuwin Current is always a surface current and has beneath it an equatorward undercurrent (Godfrey and Ridgway, 1985; Griffiths and Pierce, 1986; Smith et al., 1991; Morrow et al., 2003). Additionally, these other examples are *countercurrents* which exist in addition to the normal broad, slow eastern boundary current flow. Along the western coast of Australia, however, there is no regular, continuous equatorward surface flow within 1000 km of the coastline and there is no persistent upwelling along the coast (Smith et al., 1991).

The Leeuwin Current flows poleward as a relatively strong and narrow jet along the outer edge of the continental shelf off western Australia. It is ~50 km wide, exists in the upper 250 m of the water column, and averages ~30 cm s^{-1} with a seasonal maximum of ~60 cm s^{-1} (Schott and McCreary, 2001). A series of eddies develop on the seaward side of the current (Griffiths and Pierce, 1986; Smith et al., 1991; Batteen and Butler, 1998; Meuleners et al., 2008). The current carries a relatively warm and low salinity water mass formed from the tropical waters off northwestern Australia (Thompson, 1984; Ridgway and Condie, 2004). There is both a local temperature maximum and salinity minimum along the core of the current (Smith et al., 1991). Below a depth of ~300 m, a more saline undercurrent flows toward the equator just offshore of the continental shelf break (Schott and McCreary, 2001; Morrow et al., 2003). The Leeuwin Undercurrent (LU) carries an equatorward mass transport comparable to the poleward transport of the surface current (Godfrey and Ridgway,
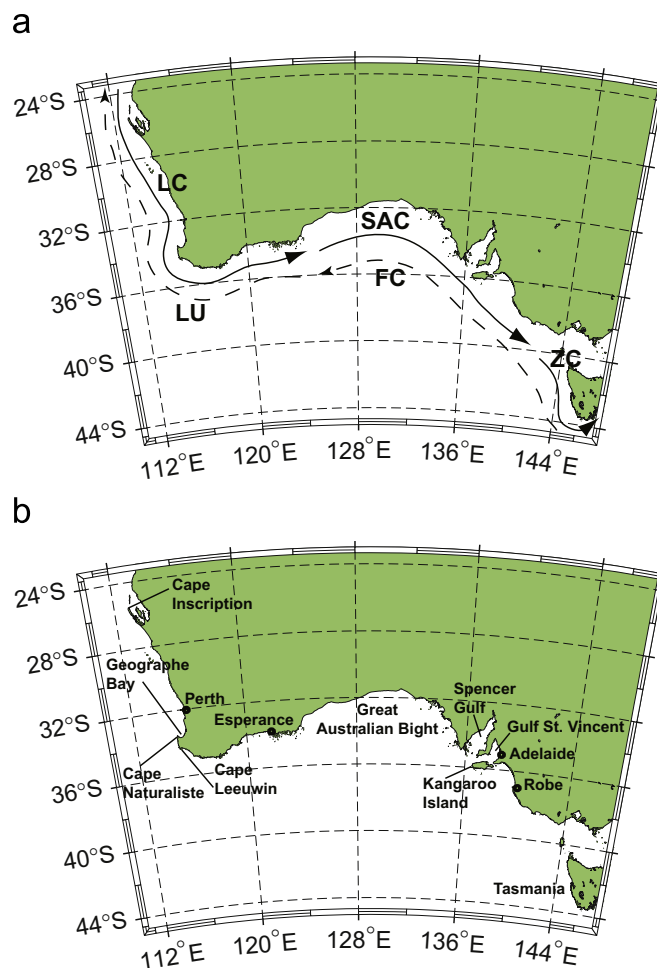
Fig. 1. (a) Schematic of large-scale currents and undercurrents off the western and southern coasts of Australia consistent with suggested naming convention of Ridgway and Condie (2004) (see the text for smaller-scale currents such as the Ningaloo and Capes Current.); (b) Geographical names for locations in the study area.

1985). The speed of the undercurrent is about one-third that of the surface current with a mean velocity of ~10 cm s^{-1} at 450 m depth (Smith et al., 1991).

The sea level drops about one-third of a meter between 20°S and 32°S (Thompson, 1987), which is a far greater sea-level gradient than in the Atlantic and Pacific Oceans (Schott and McCreary, 2001). There is general agreement that the pressure gradient arising from this anomalously large steric height difference is the principal forcing mechanism of the Leeuwin Current (e.g., Thompson, 1984; Godfrey and Ridgway, 1985; McCreary et al., 1986). Even though there is a strong equatorward component to the wind stress year-round, this pressure gradient is strong enough to overwhelm the wind forcing and generate a poleward surface current (Smith et al., 1991).

The Leeuwin Current accelerates as it flows farther south and converges to a width of ~20 km between Cape Naturaliste and Cape Leeuwin (see Fig. 1b for locations of geographical names), where it reaches its maximum speed of ~70 cm s^{-1} (Cresswell and Golding, 1980). In this area, the front separating the warm waters of the current from the colder offshore waters becomes much stronger and sharper, with sea surface temperature in the current as high as 21 °C in contrast to the offshore water of 15 °C (Griffiths and Pierce, 1986). The flow hugs the shelf break around the bend of Cape Leeuwin and flows eastward along the southern coast as

far east as the Great Australian Bight (Godfrey and Ridgway, 1985; Griffiths and Pierce, 1986; Godfrey et al., 1986; Rochford, 1986; Ridgway and Condie, 2004). This flow remains a continuous flow as the Leeuwin Current and the primary forcing mechanism appears to be the pressure gradient, even though winds along the southern coast become westerly, aligned with the flow of the current.

Though the Leeuwin Current is always poleward off the west coast, the strength of the flow is highly seasonal with the strongest flow in winter when the opposing winds are weakest (McCreary et al., 1986; Batteen and Butler, 1998). The seasonal variability appears to depend almost completely upon the variability of the wind. There is little variability in the pressure gradient (Smith et al., 1991). The location of the current appears to vary slightly with season as well. The current is relatively strong and lies along the shelf break in late summer and autumn (March–May). It is strongest and farther seaward in winter (June–August). During spring (September–December) the current is weak and again lies along the shelf break. It almost vanishes in early summer (January) (Smith et al., 1991).

The wind stress along the coast off southern Australia is predominately eastward. Variability is caused by the passage of storms and cold fronts during the winter. This downwelling favorable wind can result in an eastward coastal current which can extend from Cape Leeuwin continuously to the coast of Tasmania (Cirano and Middleton, 2004). While drifting buoy tracks have confirmed the existence of a narrow, shelf-edge coastal current extending from Cape Leeuwin across the entire distance of southern Australia (Godfrey et al., 1986), satellite sea surface temperature (SST) imagery has not been able to resolve the exact structure of the circulation due to the complexity of the SST structure (Ridgway and Condie, 2004).

The current is narrowest and has the strongest and sharpest temperature front at Cape Leeuwin. It becomes slower and broader and the front becomes weaker with increasing distance along the southern coast (Griffiths and Pierce, 1986). The current contains a series of smaller-scale eddy-like features across the Great Australian Bight (Ridgway and Condie, 2004). Along the western Bight, the water mass in the shelf-edge current changes. A warm water mass forms in a narrow strip of shallow water between 124°E and 129°E in the western Bight (Herzfeld and Tomczak, 1997; Ridgway and Condie, 2004). This water spreads eastward along the outer shelf of the Bight and is readily distinguished from the Leeuwin Current by its higher salinity. This plume is ~2–3 °C warmer than the surrounding water due to heating in the shallow region. The plume can spread eastward as far as 136°E (almost to Adelaide/Kangaroo Island area) in the summer (Herzfeld and Tomczak, 1997).

An anticyclonic gyre exists in the Great Australian Bight as this coastal current continues eastward along the shelf break while inshore of it, a westward current flows near the shore (Middleton and Platov, 2003). This westward current along the shore causes upwelling along the coast of the eastern Bight and advects cold water westward in the Bight (Herzfeld and Tomczak, 1997). This anticyclonic circulation also causes a local high in the sea level between 120°E and 130°E (Middleton and Platov, 2003). This circulation appears to be largely unaffected by surface heat fluxes and fresh water input (Middleton and Platov, 2003).

Baroclinic instability dominates the coastal areas off southern Australia (Godfrey et al., 1986; Batteen and Butler, 1998). The coastal current reaches its maximum speed of ~50 cm s^{-1} in the area offshore of Kangaroo Island where the shelf is narrowest. Offshore of this region, between the Eyre Peninsula and Tasmania, lies a complex weak eddy field. There the Flinders Current (FC) surfaces and flows toward the northwest in winter (Cirano and Middleton, 2004). Anticyclonic loops in the coastal current have been observed east of 124°E (Godfrey et al., 1986).

As the continental shelf becomes oriented more meridionally in the east, the coastal current continues to follow the shelf break poleward along the west coast of Tasmania. In this area, the current is called the Zeehan Current (Cirano and Middleton, 2004; Ridgway and Condie, 2004). This current is largely subsurface, located along the outer continental slope, and averages ~50 cm s^{-1}. In the upper 500 m of the water column, isotherms are downwelled by ~100 m. The resulting thermal wind shear is strong enough to cause an undercurrent (Middleton and Cirano, 1999).

Along the coast between Robe (~37°S, 140°E) and the eastern Bight, the mean wind stress has an equatorward (upwelling favorable) component which is particularly strong between January and March. These winds can cause significant upwelling events off the Gulfs and Robe region. The deepest upwelling occurs south of Kangaroo Island where 15 °C water is upwelled from ~150 m depth. This is one of very few areas anywhere along the southern Australian coastline where upwelling is regularly found at the surface. Upwelling has even been observed when winds are not upwelling favorable (Middleton and Platov, 2003).

Ridgway and Condie (2004) have suggested a standard naming convention for the large-scale current system of the southern coast (which will be used in this study) based on differences in geography, forcing mechanisms, and water masses. As noted earlier, a graphical depiction of these major currents using the Ridgway and Condie (2004) naming convention is included in Fig. 1a.

The flow turning around Cape Leeuwin and penetrating as far as the western Great Australian Bight is called the Leeuwin Current. The section of the flow from the Bight to Bass Strait is called the South Australia Current (SAC), a name that was found in atlases dating back as far as 1853. This section of the current contains the salty water mass formed in the Bight. It is broader than the Leeuwin Current, and appears to be forced more by local winds than the pressure gradient. Finally, the Zeehan Current (ZC) is that southward flowing, warm, saline current along the west coast of Tasmania. Undercurrents in the region flow in the opposite direction from the coastal currents.

The undercurrent flows northward along the coast of Tasmania and then westward along the eastern South Australia coast and across the Great Australian Bight. In this area it is called the Flinders Current (Cirano and Middleton, 2004). The undercurrent continues westward from the Great Australian Bight to Cape Leeuwin where is named the Leeuwin Undercurrent. The undercurrent flows at ~one-third the speed of the surface current at ~10 cm s^{-1} (Middleton and Cirano, 1999). It has a winter maximum of ~16 cm s^{-1} at a depth of ~400 m (Middleton and Cirano, 2002).

There is considerable interannual variability in the Leeuwin Current along the west coast of Australia (Deng et al., 2008). The strength of currents along the southern coast is highly dependent upon the winds. The high pressure cell over the continent (which drives the westerly winds along the southern coast) is also known to have interannual variability which could lead to large variability in the current system along the southern coast (Ridgway and Condie, 2004). To date, the degree of variability remains unknown.

1.2. Modeling background

Most large-scale modeling studies of the Leeuwin Current System (LCS) have been investigations off the western coast of Australia (McClatchie et al., 2006a). Thompson (1987)

investigated why, in the presence of upwelling favorable winds, the flow was poleward and no upwelling was observed. Weaver and Middleton (1989) used a closed basin Bryan-Cox general circulation model to investigate mechanisms for the generation of the Leeuwn Current. Batteen and Rutherford (1990) investigated the role of thermally forced gradients in the generation of the Leeuwin Current, the undercurrent, and its eddies, while Batteen et al. (1992) investigated the additional effects of annual climatological wind forcing on the Leeuwin Current System.

In more recent large-scale studies, the Leeuwin Current System domain was extended to include both the western and south-western coasts of Australia, as far across as Esperance (122.5°E). Batteen and Butler (1998) examined the effects of continuously forced annual Indian Ocean thermohaline gradients on the currents and eddies of the Leeuwin Current System in the absence of topography. Batteen and Huang (1998) investigated the effect of salinity on the density driven flow and found that both the temperature and salinity are required to accurately characterize the large-scale circulation of the Leeuwin Current System. Batteen et al. (2007a) investigated the generation of eddies with the addition of bottom topography in the Leeuwin Current System off western and southwestern Australia.

In addition to the larger scale studies, there have been smaller-scale regions modeled for the Leeuwin Current System. Meuleners et al. (2007) have modeled the Leeuwin Current System between Carnarvon (25°S) and Jurien Bay (36°S). Rennie et al. (2007) have modeled the surface and subsurface currents in the Leeuwin Current System between 28°S and 36°S.

Large-scale modeling studies of the southern coast have not been extended to include the western coast of Australia. An idealized representation of the Great Australian Bight was modeled to investigate the seasonal cycle of sea surface temperature (Herzfeld and Tomczak, 1997). Middleton and Cirano (2002) used an idealized numerical model to examine the Flinders Current, with simple geometry and topography, and did not include horizontal variations in density. The mean summertime shelf circulation of Australia's southern shelves was examined by Middleton and Platov (2003). The model domain extended from ~120°E across to the western coast of Tasmania and included western Bass Strait. The winter shelf and slope circulation was investigated by Cirano and Middleton (2004) over a region extending from ~120°E across to the eastern coast of Tasmania and included the whole of Bass Strait. The latter two studies involved a high-resolution numerical model nested inside of a global circulation model, and incorporated seasonally averaged forcing mechanisms.

1.3. Objective

While the unique character of the coastal current system off the western and southern coasts of Australia has been recognized (Ridgway and Condie, 2004), this vast 5500-km-long boundary flow has been studied far less than other current systems of the world (Herzfeld and Tomczak, 1997; Middleton and Cirano, 1999, 2002; Ridgway and Condie, 2004). Recent observational studies from satellite altimetry and climatology (Ridgway and Condie, 2004) are consistent with a continuous current extending from its origin at the North West Cape to the southern tip of Tasmania. As stated earlier, satellite SST imagery has not been able to resolve the exact structure of the circulation due to the complexity of the SST structure (Ridgway and Condie, 2004).

This study seeks to extend prior large-scale efforts by using a domain that encompasses the western coast of Australia, the Great Australian Bight, and the western coast of Tasmania, allowing a better understanding of this 5500 km

coastal region. Previous coastal modeling studies have focused on either the western Australian coast to Esperance or on southern Australia.

This modeling study of the entire region will allow the systematic exploration of the two forcing mechanisms (i.e., wind-forcing and thermohaline gradients) and their interactions. Ridgway and Condie (2004) have noted that the intriguing aspect of the current system is that the two independent forcing mechanisms act in a synergistic manner such that the longest continuous coastal current system in the world is maintained. The study uses a large-scale, eddy resolving, regional circulation model (in this case the Princeton Ocean Model (POM)) of the entire region to systematically address the roles the forcing mechanisms can play in generating and maintaining the major features of this continuous coastal current system of the entire circulation off western and southern Australia.

While observations provide insight for the basic nature of features in the coastal current system, process-oriented studies are useful for systematically investigating the characteristics and dynamical forcing mechanisms for the currents and eddies in the current system. The results of these investigations should ultimately provide insight for interpreting observations and remotely sensed data in the region (e.g., Ridgway and Condie, 2004). The basic approach in carrying out the experiments has been to change only one parameter for each case. By comparing and contrasting the results of each experiment, we gain a better understanding of which type of forcing or combination of forcing is responsible for producing each of the main features of the current system off western and southern Australia.

This study of the entire current system off western and southern Australia is organized as follows. Section 2 provides a brief description of the model, data sets and open boundary conditions. A series of process-oriented experiments (Section 3), arranged in order of increasing complexity (see Table 1), seeks to isolate which features in the current system are caused by which type of forcing. The complexity of the modeling studies is further explored by adding seasonal (Section 4) and then daily varying winds (Section 5) to isolate the effects of temporal variability as well as using higher spatial resolution wind forcing to examine features generated by smaller-scale wind features. Summary remarks are presented in Section 6. Note that additional figures in support of the experiments are presented as supplemental material.

2. Model description, data sets and open boundary conditions

The POM, a well-documented (e.g., Blumberg and Mellor, 1987; Mellor, 2004) sigma-coordinate model was used for the modeling portions of this study. POM is a primitive equation, free-surface model with a second-moment turbulence closure scheme (Mellor and Yamada, 1982) that can realistically simulate processes associated with continental shelf flows and bottom boundary layer dynamics in coastal regimes.

The horizontal grid resolution varies from 5.7 km by 6 to 13.7 km by 10.2 km. The varying resolution allows for more grid points in areas of larger gradients (of temperature and bottom topography) and fewer grid points in areas with smaller gradients. The model uses 21 vertical sigma levels which are most closely spaced near the surface and the bottom in order to better resolve the surface and bottom boundary layers, both of which are important in coastal regions. All choices for processes and values used in the model are the default POM parameters (see Mellor, 2004) unless specifically prescribed (see Miller (2006) for a more complete description of model choices, preprocessing and experiments).

Table 1
Summary of experimental design showing climatology (temperature and salinity forcing), wind forcing, and bottom type for each experiment.

| Experiment	Climatology	Wind	Bottom type
1	Horizontally averaged annual	Annual	Flat bottom
2	Horizontally averaged annual	Annual	Smoothed topography
3	Full annual	None	Flat bottom
4	Full annual	None	Smoothed topography
5	Full annual	Annual	Flat bottom
6	Full annual	Annual	Smoothed topography
7	January	Summer	Smoothed topography
8	July	Winter	Smoothed topography
9	July	Higher resolution daily July 2001	Smoothed topography
10	January	Higher resolution daily January 2001	Smoothed topography
11	January	Higher resolution daily January 2000	Smoothed topography
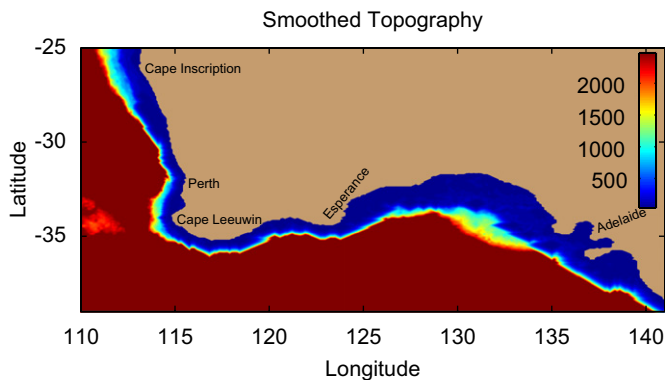
Fig. 2. Model domain and bottom topography. The model domain extends from 22.5°S to 40°S and from 107.5°E to 142.5°E. The topography was first smoothed with the one-dimensional direct-iterative smoothing method of Martinho and Batteen (2006), then all depths greater than 2500 m were reassigned a depth of 2500 m.

2.1. Data sets

The model domain (Fig. 2) contains most of the western and southern coasts of Australia, from 22.5°S to 40°S and 107.5°E to 142.5°E. The topographic data was obtained from the Institute of Geophysics and Planetary Physics, University of California San Diego (Smith and Sandwell, 1997). This topography data set, with a resolution of 2 min, was compiled from over 30 years of bottom echo sounding by ships. Gravity estimates derived from altimetry data were used to interpolate soundings in data sparse regions.

A new topography smoothing technique (Martinho and Batteen, 2006) was used, which preserves the original configuration of the coastline, continental shelf break, seamounts, and islands, while still reducing the slope parameter to an acceptable value at all grid points. According to Mellor et al. (1998), the slope parameter must be less than 0.2 at all locations in order to decrease the pressure gradient force error to an acceptable error (i.e., ~0.5 cm s^{-1}). This smoothing technique uses an iterative, one-dimensional smoothing method, and has been successfully used in the modeling of the coastal Canary and Iberian current system (Batteen et al., 2007b).

The annual temperature and salinity climatology data set from the World Ocean Atlas 1994 (WOA94) (Levitus and Boyer, 1994; Levitus et al., 1994) was used to initialize the model for the annual thermohaline experiments (see Table 1). The annual temperature fields for the surface are shown in Fig. 3a. WOA94 monthly temperature and salinity fields were also used for the seasonal and daily wind-forcing experiments (see Table 1). The January (July) temperature fields for the surface are shown in Fig. 3b (3c).
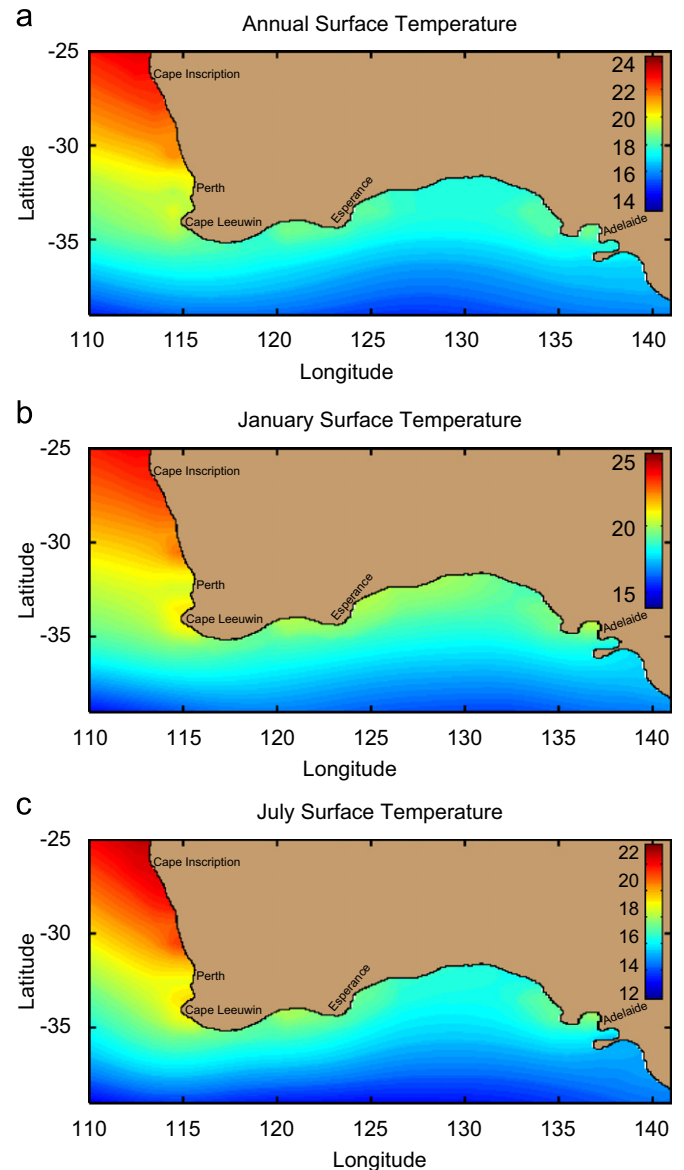

Fig. 3. Annual (a), January (b) and July (c) climatological surface temperature (°C) obtained from Levitus and Boyer (1994).

The European Center for Medium-range Weather Forecasting (ECMWF) daily climatological winds were averaged over time in order to obtain the annual, January, and July non-weighted average wind vector fields (Fig. 4a–c) used for the annual, January
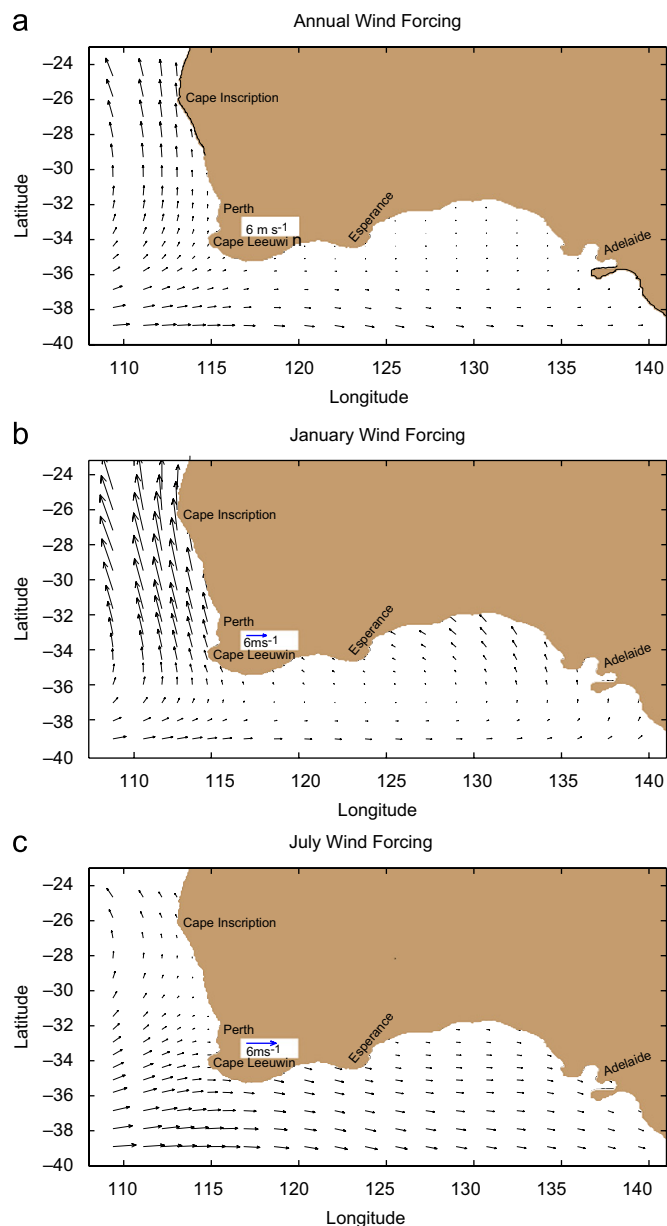
a

Annual Wind Forcing

b

January Wind Forcing

c

July Wind Forcing

Fig. 4. Wind stress vectors in m/s calculated from annual (a), January (b) and July (c) climatological ECMWF winds obtained from Trenberth et al. (1990). Length of arrow in white rectangle equals 6 m/s. (For interpretation of the references to colour in this figure legend, the reader is referred to the web version of this article.)

and July wind-forcing experiments, (see Table 1). The wind fields for the higher spatial resolution daily wind experiments (see Table 1) were formed from the Navy's Operational Global Atmospheric Prediction System (NOGAPS) model operational analysis. This data set is provided as a part of the Global Ocean Data Assimilation Experiment (GODAE). These winds are reanalyzed to a 1° by 1° horizontal grid (Goerss and Phoebus, 1992). The NOGAPS winds were used for each day of June 2001 through August 2001 (Experiment 9), December 2000 through February 2001 (Experiment 10), and December 1999 through February 2000 (Experiment 11).

2.3. Open boundary conditions and volume constraint

Open boundary conditions are a necessity for each of the component forcings. As a result, there is no coupling to output

from a general circulation model. Although no general criteria can determine the best boundary conditions for a specific model or study, correct specification of the open boundary conditions is imperative for achieving realistic results. Otherwise reflections, spurious currents, and/or changes in the total water volume in the model can occur. For free-surface models, such as this one, it is important that the boundary conditions be transparent to the waves. In this model, a zero gradient boundary condition (Chapman, 1985) is used for the elevation. This boundary condition assumes that the phase speed is infinite. The boundary values can evolve in time. The condition also allows geostrophic flow normal to the boundary. For the baroclinic velocity components normal to the boundary, an explicit wave radiation scheme based on the Sommerfeld radiation condition is used. For inflow situations, the model is forced with WOA94 (Levitus and Boyer, 1994; Levitus et al., 1994) temperature and salinity values and an advection scheme is used for outflow situations.

For the barotropic velocity components, Flather (1976) developed a radiation condition, based on the Sommerfeld equation combined with the continuity equation, which allows radiation of wave energy across the boundary while allowing conservation of mass inside the model domain. Recently Leth and Middleton (2004) and Middleton and Leth (2004) adopted the Flather condition as a backward open boundary condition to model the flow poleward of the equatorward open boundary. In their case, use of the Flather condition fortuitously simulated the vanishing of the mean summer wind field at 26°S, which is the geographical origin for steady summer wind-forced flow on the west coast of South America. The adoption of 22.5°S using the same Flather condition for western Australia raises concerns for studies that use steady wind-forced flow. In particular, the wind-forced flow may be unduly large or small.

Palma and Matano (1998) reformulated the Flather scheme using the Roed and Smedstad (1984) technique, which breaks the velocity into both global and local components. Note that this open boundary condition, called the Flather radiation plus Roed local solution by Palma and Matano (1998), was used in our experiments. Palma and Matano (2000) showed good results with this boundary condition during tests to determine the boundary condition's response to an alongshelf wind stress. Palma and Matano (1998) also showed that the boundary condition demonstrated good reflection properties and results in a test that determined the boundary condition response to the combined action of wind forcing and wave radiation. Their tests were executed with the barotropic version of POM and compared well with benchmark results using cyclic boundary conditions or expanded domains.

An additional modeling improvement that has more realistically maintained classical eastern boundary current features when open boundary conditions are used (which do not conserve volume) has been the implementation of a volume conserving scheme proposed by Marchesiello et al. (2001) and used by Batteen et al. (2007a, b). Experiments with and without the scheme showed that when there was no volume constraint, a spurious poleward flow could be generated at the equatorward open boundary, which by day 90 for the Canary Current system extended from south to north along the entire model domain (Hopkins, 2006).

3. Process-oriented experiments

Several process-oriented experiments, arranged in order of increasing complexity (see Table 1) are explored. Each experiment is run on a beta-plane and with the irregular coastline shown in Fig. 2. For each experiment, following the description of the

modeled features and their locations, possible mechanisms for their generation and observational support for the modeled features and locations are presented.

In Experiment 1(Experiment 2) the horizontally averaged annual climatology is used with annual wind forcing on a flat bottom (with topography). Experiment 3 (Experiment 4) investigates the effect of thermohaline gradient forcing by using full annual climatology and no wind forcing on a flat bottom (with topography). Experiment 5 (Experiment 6) includes both wind and thermohaline forcing mechanisma on a flat bottom (with topography) to gain an understanding of the combined effect of the forcing mechanisms on the dynamics of the 5500-km-long coastal system.

For the annual wind-forcing experiments (Experiments 1, 2, 5 and 6 in Table 1)), the model was forced from rest with the annual ECMWF wind fields (e.g., Fig. 4a), which were interpolated to the model grid. Model runs using horizontally averaged climatology (Experiments 1 and 2 in Table 1) use the same initial temperature and salinity over the entire model domain (e.g., 19.8 °C and 35.4 are the temperature and salinity values, respectively, for the surface) to remove any thermohaline gradient forcing. For the annual thermohaline experiments (Experiments 3–6 in Table 1), the model was initialized with annual temperature (e.g., Fig. 3a) and salinity (not shown). Since the model runs reached a quasi-equilibrium state (i.e., where the total kinetic energy is nearly constant which corresponds to the spin-up time of the basin shelf circulation) in a relatively short time (~26 days), zero salinity and temperature fluxes were prescribed at the ocean surface.

3.1. Wind forcing over a flat bottom

In Experiment 1, the model was initialized using horizontally averaged annual temperature and salinity climatology, which removes all thermohaline forcing. A flat bottom with a uniform depth of 2500 m eliminated any topographic effects. The sole forcing in this experiment was from the annually averaged climatological winds.

The goal of this experiment was to highlight the role of wind forcing and its variability (including wind stress curl) on a beta-plane off the western and southern coasts of Australia. This wind field (Fig. 4a) is southerly (i.e., equatorward) along the entire western coast of Australia and the wind increases in magnitude toward the north. Over the coastal waters off southern Australia, the winds are westerly, except inside the Great Australian Bight, where the winds are relatively weak and southerly. The stronger offshore winds decrease in strength toward the coast, resulting in a positive wind stress curl along the entire southern coastline. This should result in the generation of a westward current, consistent with Middleton and Cirano (2002).

As expected, a coastal surface current flows westward and hugs the coastline along the entire length of southern Australia, resulting in a continuous surface current that begins relatively weak (~2 cm s^{-1} at ~140°E), strengthens as it flows toward the west (~10 cm s^{-1} at ~130°E), and rounds the bend of Cape Leeuwin (where it reaches a speed of ~12 cm s^{-1}). It then flows equatorward with broad offshore flow from ~55 km wide off Cape Leeuwin to ~130 km wide off 26°S (Fig. 5).

The equatorward winds along the west coast, as expected for winds favorable for upwelling, induce net offshore surface Ekman transport, generating regions of upwelling evidenced by the cool water along the coast at day 60 from ~29°S to the northern end of the model domain (Fig. 5). As expected, the coastal upwelling and its offshore extent have intensified with time along the west coast (not shown). The more intense upwelling in the north is associated with the stronger winds in the north. Along the
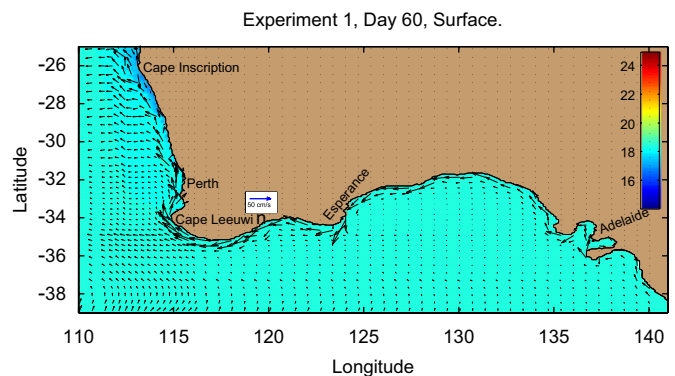

Experiment 1, Day 60, Surface.

Fig. 5. Experiment 1 day 60 sea surface temperature (°C) and velocity vectors. Length of arrow in white rectangle in Fig. 5 and other horizontal plots with velocity vectors is 50 cm/s. (For interpretation of the references to colour in this figure legend, the reader is referred to the web version of this article.)

southern coast of Australia, upwelling is not readily discernible (Fig. 5), as expected due to the relatively weak winds along the coast (Fig. 4a).

Off the west coast, a relatively weak poleward undercurrent develops below the coastal equatorward current. For example, at 26°S, the core of the undercurrent flows at ~7 cm s^{-1} at a depth of ~150 m (not shown). Farther south, at Cape Leeuwin (~34°S), the undercurrent is weaker and deeper: ~2 cm s^{-1} at ~350 m depth (not shown). Along the southern coast a relatively weak undercurrent with a core depth of ~1 cm s^{-1} at ~250 m depth develops in time at the coast below the core of the relatively broad and deep westward surface current (not shown).

The generation of a poleward undercurrent along the west coast is consistent with previous process-oriented modeling studies which have shown that a poleward undercurrent can be generated due to meridional variability in the predominantly equatorward wind stress (Batteen et al., 1989) and/or to the planetary beta effect (e.g., McCreary et al., 1986; Batteen, 1997). The beta effect allows the existence of freely propagating planetary waves, i.e., Rossby waves (Gill, 1982). The offshore propagation of these waves contributes to the generation of an alongshore pressure gradient field, which can aid the development of subsurface currents along the eastern boundary. In time the surface current can widen and subsequently move away from the coast, causing the undercurrent to intensify and extend closer to the surface. As a result, the beta effect can change both the vertical and horizontal structure of the surface and subsurface currents.

The west coast results from this experiment resemble the dynamic characteristics associated with classical eastern boundary currents where wind is the predominant forcing mechanism, on a beta-plane. These classical features include the generation of coastal surface currents in the direction of the wind along with upwelling due to favorable winds. Consistent examples of observational support for such currents on the west coast are the Ningaloo Current observed in a summertime cruise from 22°S to 24°S (Woo et al., 2006) and the Capes Current observed between November and March between 32°S and Naturaliste (Pearce and Pattiaratchi, 1999). The Cresswell Current off the southwest coast has been postulated by McClatchie et al. (2006a) to also be a wind-driven westward coastal current in the summertime.

Unlike the coastal current on the west coast which broadens with time due to the planetary beta effect, the coastal current on the southern coast is trapped to the coast and also increases in magnitude as the current flows westward (Fig. 5). This trapping

and increase in magnitude westward is consistent with the dynamic characteristics associated with the generation of a westward surface current due to positive wind stress curl. In the austral summer the locations of two westward flows rather than one off the southern coast, i.e., a coastal current and the Flinders Current, have been depicted in Fig. 2 of Middleton and Bye (2007). Middleton and Cirano (2002) have shown that a positive wind stress curl on the southern coast can generate the westward Flinders Current, which has been observed to lie off the continental slope as a subsurface current which can reach the surface. Here, due to the absence of topography, the coastal current and the Flinders Current remain indistinguishable and appear as one relatively broad and deep westward surface flow trapped at the coast (not shown). This emphasizes the key role that topography plays in separating the westward flow into two separate cores (see below).

3.2. Wind forcing over topography

Experiment 2 (see Table 1) mimics Experiment 1, except that, instead of a flat bottom, topography has been incorporated. A primary goal of Experiment 2 is to investigate the effects of topographic beta and demonstrate its role in a wind-forced model of the western and southern coasts of Australia.

Like Experiment 1, an equatorward (westward) surface current develops along the west (southern) coast (Fig. 6a). The current is stronger along the west coast than the southern coast of the model domain due to the stronger winds off the west coast (Fig. 4a). A new feature is that the currents are stronger on the shelf region than at the coast (compare Figs. 6a and 5). This is due to the trapping effect of bottom topography.

In the flat-bottom experiment (Experiment 1) upwelling could occur along much of the west coast (Fig. 5). Here, in areas where upwelling is present (e.g., off capes such as Cape Inscription), the upwelling can be more intense, which can be a precursor to upwelling centers. The results (Fig. 6a) also show that, even with upwelling favorable winds, topography can hinder the development of some upwelling regions (e.g., in coastal embayments).

A typical cross-section of meridional velocity, at 26°S, off the west coast (Fig. 6b) shows that in addition to a core at the coast due to the wind forcing, there is another core of the equatorward surface current centered over the shelf break. This illustrates that in broad shelf regions (e.g., Fig. 6b) topography can play a role in separating the equatorward flow into separate cores, one at the coast and one over the shelf.

On the southern coast topography also plays a role in trapping the relatively broad and deep core of the surface western coastal current over the shelf break and continental slope (e.g., Fig. 6c) rather than at the coast (not shown). Note that the core of the current has its greatest magnitude below the surface (e.g., of ~40 cm/s between ~100 and 700 m depth at 117°E) rather than at the surface. The location of a subsurface core off the continental slope is consistent with observations of the Flinders Current. The result here shows that positive wind stress curl, which generates a westward current, and topography, which has a trapping effect over the shelf due to topographic beta, can play a combined role in generating features consistent with the Flinders Current.

3.3. Thermohaline forcing over a flat bottom

Experiment 3 (see Table 1) focuses on the thermohaline gradient. The model is initialized with full annual temperature (Fig. 3a) and salinity (not shown) climatology that has not been horizontally averaged. A flat bottom (constant depth of 2500 m) is used to isolate the combined effect of thermohaline forcing from
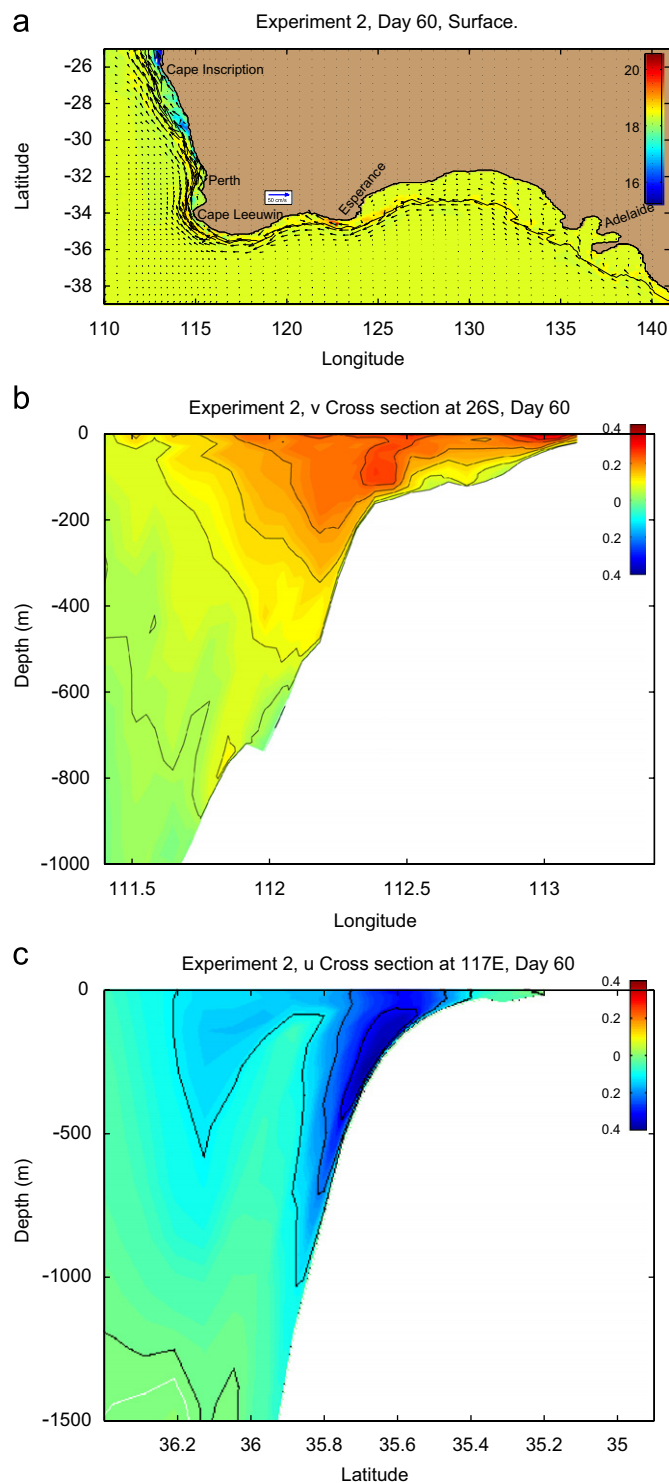
Fig. 6. Experiment 2, day 60 (a) sea surface temperature (°C) and velocity vectors; (b) cross-section of meridional velocity component (m s^{-1}) at 26°S; and (c) cross-section of zonal velocity at 117°E. Note that in (b) and all cross-section plots, the maximum current speed for that latitude or longitude is used as the current speed in that location. In (b) and all meridional cross-sections, red is equatorward (north) and blue is poleward (south). In (c) and all zonal cross-section of zonal velocity plots, red is eastward and blue is westward. The white contour is zero. (For interpretation of the references to colour in this figure legend, the reader is referred to the web version of this article.)

bottom topopgraphy. There is no wind forcing. A primary goal is to highlight the effects of thermohaline forcing off the western and southern coast of Australia.

The annual climatological surface temperature (Fig. 3a) shows a strong north–south gradient with a maximum temperature of ~24 °C along the western coast of Australia at the northern end of the domain and decreasing values to the south to a minimum of ~14 °C at the southern edge of the model domain. The climatological surface salinity (not shown) reaches a maximum of ~35.8 at the center of the western edge of the model domain and decreases slightly to both the north and south.

In contrast to the previous experiments, a relatively energetic and dynamic current develops (not shown). The flow is poleward along the entire western coast of Australia, extends eastward around Cape Leeuwin into the Great Australian Bight and continues poleward as far east as Kangaroo Island by day 30. The strength of the surface current is created by the large alongshore thermohaline gradient, which generates a relatively strong onshore geostrophic inflow. As the inflow nears the coast, it is deflected southward creating a relatively narrow core of warm water along the entire coast of western Australia. As the current rounds Cape Leeuwin, it is steered eastward due to the Coriolis effect (to the left in the Southern Hemisphere). The surface current has advected relatively warm water well south of Cape Leeuwin, and then as far east as Esperance by day 30 (not shown).

In addition to strong surface currents, relatively intense undercurrents are established adjacent to the coastline. A typical cross-section of zonal velocity along the southern coast (Fig. 7a) shows the core of the westward undercurrent centered at ~600 m depth with a speed of ~35 cm/s underlying the eastward surface current with a core speed of ~55 cm/s at day 30.

The horizontal temperature gradient and the increased strength of the current (not shown) produce large horizontal shear, resulting in an enhancement of barotropic instability. The relatively strong surface current and the intense undercurrent (e.g., see Fig. 7a) also produce large vertical shear, resulting in an enhancement of baroclinic instability. As a result of both barotropic and baroclinic instability, large meanders develop along the west and southwest coast (not shown). In time near Cape Leeuwin cold, sub-polar water is entrained west of the main flow resulting in the generation of dipole eddy pairs (not shown). Due to the effects of planetary beta, the current along the western coast broadens over time.

The generation of a relatively strong, poleward surface current (of ~100 cm/s) overlying an equatorward undercurrent (of ~25 cm/s) off the west coast (not shown) demonstrates the importance of relatively strong climatological thermohaline gradients. The direction of the currents is consistent with observations of the Leeuwin Current and Leeuwin Undercurrent. Off the southern coast, the eastward direction of the surface current is consistent with the Leeuwin Current with slightly decreasing magnitudes as it propagates eastward, i.e., from ~55 cm/s at 117°E (Fig. 7a) to ~50 cm/s at 130°E (Fig. 7b). Note that the direction of the Leeuwin Current at 130°E is indistinguishable in this experiment from another surface current, called the South Australian Current (see Fig. 1a), using the naming convention of Ridgway and Condie (2004).

The results of this experiment highlight that a current consistent with some of the features of the Flinders Current can be generated solely by thermohaline forcing, which is a new result. In particular the westward direction of the undercurrent along with the subsurface location of its core, and its speed off the southern coast is consistent the Flinders Current. Fig. 7a and b illustrate a core of the Flinders Current evident at ~850 m depth with a core speed of ~10 cm/s at 130°E (Fig. 7b) which intensifies in magnitude towards the west with a core speed of ~35 cm/s at ~600 m depth at 117°E (Fig. 7a). Noting that the core of the undercurrent continues to decrease to ~25 cm/s at 34°S off the west coast (not shown), the results are consistent with the
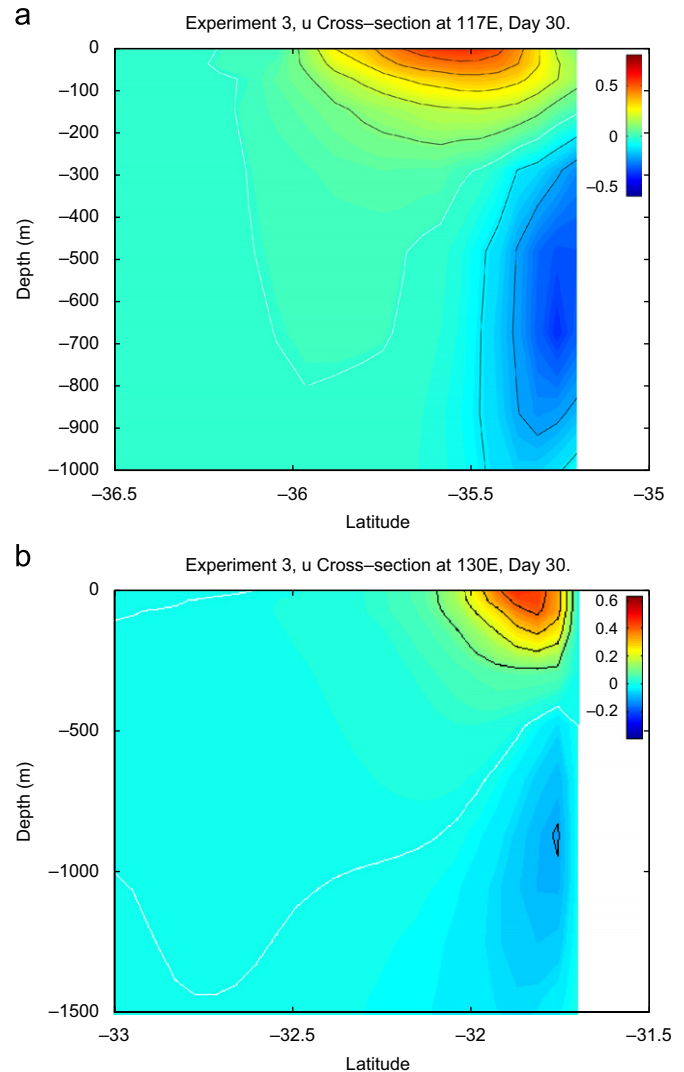

Fig. 7. Experiment 3, day 30 (a) cross-section of zonal velocity component (m s⁻¹) at 117°E, and (b) cross-section of zonal velocity component (m s⁻¹) in the Great Australian Bight (130°E).

Flinders Current providing the source waters off the southwest coast (e.g., Fig. 7a) for the Leeuwin Undercurrent. The Leeuwin Undercurrent and the Flinders Current remain indistinguishable in this experiment in terms of sharing a similar direction and core speed, particularly off the southwest coast (e.g., Fig. 7a). In this region both naming conventions have been used (e.g., by Ridgway and Condie, 2004 and by McClatchie et al., 2006a).

3.4. Thermohaline forcing over topography

Experiment 4 (see Table 1) mimics Experiment 3, except instead of a flat bottom, topography is added. The goals of Experiment 4 are to isolate the effects of topographic beta and to demonstrate its role in a thermohaline-forced model.

A poleward (eastward) current has developed by day 30 (not shown) along the west (southern) coast along with several meanders along the west and southwest coasts of Australia. Due to the bottom topography, the current remains anchored to the continental shelf/break at all locations, with no indications of continuous broadening and moving away from the coast which occurred in the flat-bottom experiments.

Off the west coast, an equatorward undercurrent opposes the poleward surface current and increases in magnitude from north

to south from ~15 cm/s with a core at ~750 m depth at 26°S (not shown) to ~20 cm/s with a shallower core depth of ~650 m depth at 34°S by day 30 (not shown), which is maintained from Cape Leeuwin to ~117°E (not shown). At 130°E, near the origin of the undercurrent, the undercurrent weakens to a speed of ~5 cm/s with a weak core at ~850 m depth adjacent to the slope (not shown). In this area, the westward flow is very broad and disorganized, unlike the strong core found farther west.

Off the west coast, the strength of the surface current is created by the large north–south thermohaline gradient. The thermohaline gradient generates a strong onshore geostrophic inflow. As the inflow nears the coast, it is deflected southward creating a narrow core of warm water along the entire coast of western Australia. Coriolis force steers the surface current around Cape Leeuwin and across the Great Australian Bight. Continual onshore flow augments the surface flow throughout the model's duration to enable the surface flow to continue along the entire coast such that poleward surface flow is discernible along the western coast of Tasmania by day 60 (Fig. 8). This continuous surface flow all along the 200 m shelf break of the 5500 km domain is consistent with Condie and Ridgway's (2004) description of the Leeuwin Current System.

The vertical shear caused by the strong, poleward surface current and equatorward undercurrent creates large meanders in the surface current (not shown), particularly along the west coast. Eddies subsequently develop so that by day 60 (Fig. 8) there are numerous eddies in different stages of development along the west and southwest coasts. Near Cape Leeuwin cold, sub-polar water has been entrained west of the main flow generating dipole eddy pairs. These detached eddies subsequently propagate westwards, consistent with the planetary beta effect, as they are no longer under the influence of topography (not shown).

The addition of bottom topography (topographic beta) isolates and traps the unique thermohaline gradient driven, surface current over the continental shelf/slope system all along the coast. Topography aids the development of realistic eddies and dipole pairs. Overall, the results of this experiment more closely resemble the distinct dynamical features that set this region apart from classical eastern boundary currents.

3.5. Wind and thermohaline forcing on a flat bottom

The final flat-bottom experiment, Experiment 5 (see Table 1) uses both wind and thermohaline forcing. In particular, the model is initialized with full annual temperature and salinity climatology. A flat bottom (constant depth of 2500 m) is used. Annual climatological wind forcing is added to determine which features in the current system dominate due to the combination of

wind forcing and thermohaline gradients in the absence of topographic effects.

The overall current pattern formed in this experiment is more similar to the pattern formed in the thermohaline forcing only Experiment 3 than to that of the wind forcing Experiment 1, showing that the strong thermohaline gradient has a greater effect on the coastal currents of the region than the wind. This onshore flow is deflected toward the south to form a poleward current which narrows and strengthens with distance toward the south (not shown). The current continues around the cape and eastward along the southern coast. The current advects a narrow band of warm subtropical water south along the western coast and then east along the southern coast to the Great Australian Bight. Meanders and eddies form in the current in the vicinity of Cape Leeuwin, while an eddy field forms offshore of the current along the southern coast between Cape Leeuwin and the Great Australian Bight. Note that the surface coastal current along the west coast is less than the currents which develop in Experiment 3 with only thermohaline forcing, showing that the wind forcing does counteract the thermohaline forcing to slow the currents. Except for the coastal location instead of a shelf break location, the surface current is similar to the Leeuwin Current, while the undercurrent off the west (southern) coast is similar to the Leeuwin Undercurrent (Flinders Current) (not shown).

3.6. Wind and thermohaline forcing over topography

Experiment 6 (see Table 1), includes all of the forcing mechanisms and most closely resembles the Leeuwin Current System in the annual sense. In particular, the model is initialized with full annual temperature (Fig. 3a) and salinity (not shown) climatology. Realistic bottom topography (Fig. 2) is used, and the model is forced with annual climatological winds (Fig. 4a).

A poleward (eastward) current develops along the west (south) coast by day 30, and advects relatively warm (Fig. 9) and fresh subtropical water polewards along the west coast and warm, more saline water eastwards along the southern coast. In west coast regions where the continental shelf is relatively wide such as near 26°S (not shown), the poleward surface current is found to extend as far as ~100 km offshore over the shelf break. This allows the wind forcing to dominate the flow inshore of the poleward current, generating an equatorward surface current directly at the coast. This equatorward flow, which is consistent with the Capes Current, subsequently leads to localized areas of upwelling distinguished by slightly cooler waters along the coast (Fig. 9) over the shelf.

The vertical shear caused by the strong, poleward surface current and equatorward undercurrent creates large meanders in the surface current, noticeable by day 30 (not shown), particularly
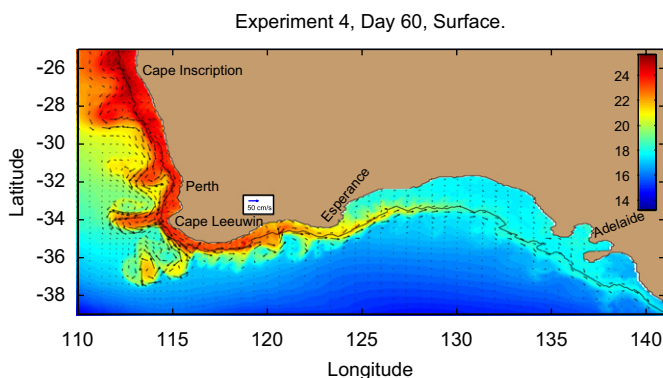

Fig. 8. Experiment 4 day 60 sea surface temperature (°C) and velocity vectors.

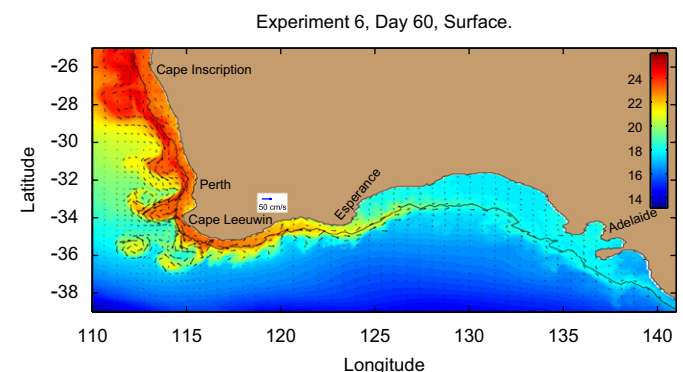**Fig. 9.** Experiment 6 day 60 sea surface temperature (°C) and velocity vectors.

along the western coast. Eddies subsequently develop so that by day 60 (Fig. 9) there are numerous eddies in different stages of development along the west and southwest coasts. Near Cape Leeuwin cold, sub-polar water is entrained west of the main flow generating dipole eddy pairs. Detached eddies propagate westwards as they are no longer under the influence of topography. The wind forcing, which opposes the poleward thermohaline induced current, can help generate better defined eddies (e.g., compare Figs. 8 and 9).

The results of this experiment, which emphasizes the combined roles of wind forcing (including its variability such as wind stress curl), thermohaline gradients and topography, show relatively realistic features as well as their locations of the Leeuwin Current System. These features include a poleward (eastward) surface current over the shelf break, an equatorward (westward) undercurrent off the continental slope, meanders and eddies offshore of the shelf break, and regions of localized upwelling along the west coast. Unlike classical eastern boundary currents, the thermohaline gradients dominate over the opposing wind forcing to drive a poleward surface current along the west coast. Even though the thermohaline gradients dominate, the wind forcing influences the development of better defined eddies and enhances the equatorward flow along the west coast in regions where the poleward surface current is farther offshore (e.g., off 26°S, Fig. 9). Bottom topography is responsible for trapping the currents over the continental slope and shelf break, thus preventing the equatorward current from dominating the surface flow.

4. Seasonal experiments

Experiments 7 and 8 are forced with both full seasonal temperature and salinity climatology and seasonal winds for January and July, respectively, in order to isolate these seasonal effects on the current system. As stated above, along the western coast of Australia, the winds are generally southerly throughout the year. The strength of these winds varies with season. During Austral summer (November through February), the southerly winds are strongest in the area between 20°S and 35°S (e.g., Fig. 4b). The winds begin to decrease in March as the monsoon over northern Australia reverses and reach a minimum in May. By July (e.g., Fig. 4c) the winds are much weaker than in summer. Throughout both seasons, the winds are westerly below ~35°S (Godfrey and Ridgway, 1985). As these winds oppose the alongshore steric sea-level slope, they are thought to be responsible for the Leeuwin Current being strongest in winter (when winds are weakest) and weakest in summer (when winds are strongest) (e.g., Godfrey and Ridgway, 1985; Smith et al., 1991).

4.1. January monthly wind and thermohaline forcing over topography

Experiment 7 (see Table 1) was the first of the seasonal wind cases and used a January monthly wind field (Fig. 4b) and the WOA94 monthly temperature (Fig. 3b) and salinity (not shown) for January. The same bottom topography (Fig. 2) and coastline from the previous experiments were used.

As expected, a broad onshore flow develops off the northern end of the western coast and is deflected toward the south as it approaches the coast, forming the poleward Leeuwin Current along the continental shelf break (Fig. 10a) which advects warm water southward along the coast, and then as far east as ~120°E by day 30 (Fig. 10a).

A new feature, not seen in the previous experiments, is the persistent presence of an equatorward shelf current lying inshore of the Leeuwin Current along the coastline along much of the western coast (Fig. 10a). For example, the equatorward shelf current is clearly visible from ~30°S to ~24°S (Fig. 10a). Beneath the poleward Leeuwin Current lies an opposing undercurrent which strengthens and deepens as it flows toward the equator (not shown).

An eastward coastal surface current lies along the western portion of the southern coast (i.e., from Cape Leeuwin to the western Great Australian Bight, Fig. 10a). In this area, the surface eastward coastal current can extend from beyond the continental shelf break all the way to the coast. At 117°E, for example, the eastward surface current has a core speed of ~38 cm s^{-1} core over the shelf break (Fig. 10b). A new feature is the presence of two cores of the westward undercurrent, both centered at ~600 m depth: a stronger core of ~28 cm s^{-1} between 36.2°S and 36°S and a weaker core of ~10 cm s^{-1} adjacent to the continental slope. The direction, speeds, and depth locations are consistent with both the Leeuwin Undercurrent and the Flinders Current. The presence of the two cores is suggestive of the stronger, wider core of the Flinders Current providing the source waters for the weaker, narrower core of the Leeuwin Undercurrent in this region.

In the eastern half of the Great Australian Bight, there is a westward coastal surface current (e.g., Fig. 10c). This is consistent with summertime observations which show that the current flow in the Great Australian Bight consists of a relatively weak gyre with the eastward South Australian Current along the shelf break, northward flow in the eastern Bight and a westward flow adjacent to the coast. For example, at 130°E (Fig. 10c) there is a westward current at the coast with a speed of ~10 cm/s. Offshore of it is an eastward current with a speed of ~21 cm s^{-1} on the shelf. Below the eastward surface current there is an opposing westward undercurrent of ~11 cm s^{-1} centered at ~700 m depth, which is consistent with the core of the Flinders Current, which increases from east to west (compare Figs. 10c and 10b).

Meanders form in the Leeuwin Current along the west coast near 30°S, near 31°S, and just south of Cape Leeuwin by day 30 (Fig. 10a), and along the western end of the southern coast between 115°E and 120°E. Eddies have formed in the Leeuwin Currrent by day 60 at ~28°S and just north of Cape Leeuwin (~33.5°S) with relatively large meanders at 31°S and southwest of Cape Leeuwin (Fig. 10d). A pool of cooler surface water upwelled by the equatorward shelf current is visible at the surface in Geographe Bay, just north of Cape Leeuwin. A continuous westward flow consistent with the South Australian Current persists across the Great Australian Bight continental shelf break with a meander/eddy field offshore of the current, consistent with observations. The gyre remains in place on the shelf of the Great Australian Bight with a westward shelf current near the coast where small patches of cooler upwelled water are discernible in the eastern end of the Bight. A slightly larger pool of upwelled water is also visible along the northern and southern coasts of Kangaroo Island (Fig. 10d).

The current system modeled by this experiment illustrates several features occurring only in the summertime. In particular there is the development of an equatorward current on the shelf inshore of the Leeuwin Current along more of the west coast than in the previous experiment. Off the southwest coast a subsurface westward undercurrent showed features consistent with both the Flinders Current and Leeuwin Undercurrent in location and velocities. The presence of two cores of the current at 117°E is suggestive of the Flinders Current supplying source waters for the Leeuwin Undercurrent in this region. Lastly the gyre/westward flow along the shore on the Great Australian Bight shelf inshore of the South Australia Current was modeled for the first time, showing that this gyre is likely a seasonal feature of
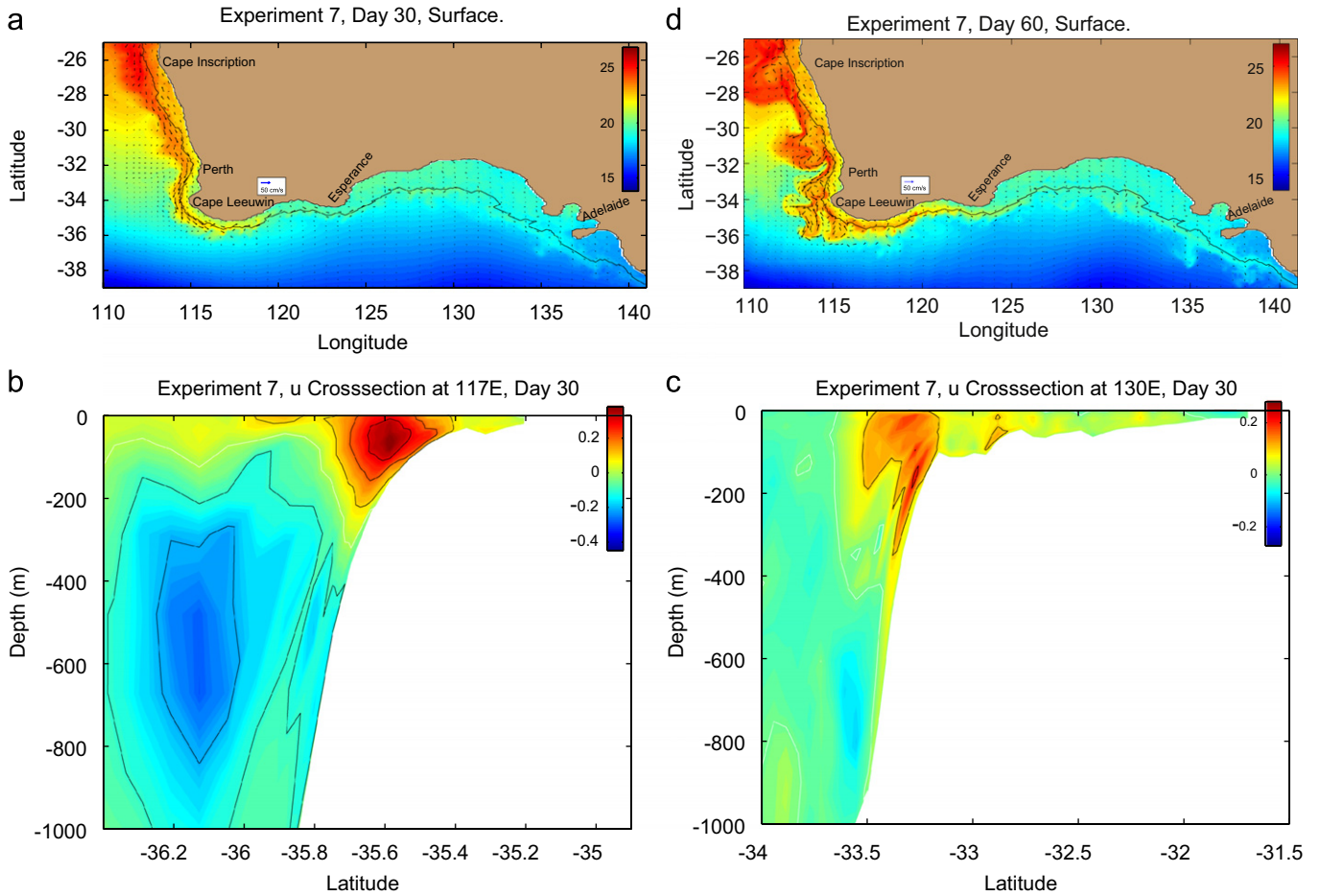
Fig. 10. Experiment 7 (a) day 30 sea surface temperature (°C) and velocity vectors (b) day 30 cross-section of zonal velocity component (m s^{-1}) at 117°E, (c) day 30 cross-section of zonal velocity component (m s^{-1}) in the Great Australian Bight (130°E), and (d) day 60 sea surface temperature (°C) and velocity vectors.

summertime, consistent with summertime observations (e.g., Godfrey et al., 1986).

4.2. July monthly wind and thermohaline forcing over topography

Experiment 8 (see Table 1) was the second seasonal wind case and used a July monthly wind field (Fig. 4c) the WOA94 monthly temperature (Fig. 3c) and salinity (not shown). The same bottom topography (Fig. 2) and coastline from the previous experiments were used.

A broad onshore flow develops off the northern end of the western coast and is deflected toward the south as it approaches the coast, forming the poleward Leeuwin Current along the continental shelf break (Fig. 11). By day 30, at 26°S the current is ~22 cm s^{-1} and ~110 km wide. It intensifies to ~40 cm s^{-1} and narrows to ~60 km wide at Cape Leeuwin (Fig. 11). An opposing equatorward undercurrent with a core speed of ~20 cm/s at ~400 m depth lies below this current adjacent to the continental slope (not shown).

The band of warm water is advected southward, then around Cape Leeuwin and eastward along the southern coast as far is ~125°E by day 30 in the western Great Australian Bight (Fig. 11). Anticyclonic meanders/eddies are discernible offshore of the current just south of Cape Leeuwin. The surface coastal current is strongest along the western end of the southern coast at ~42 cm s^{-1} at 117°E (not shown) and decreases as it flows

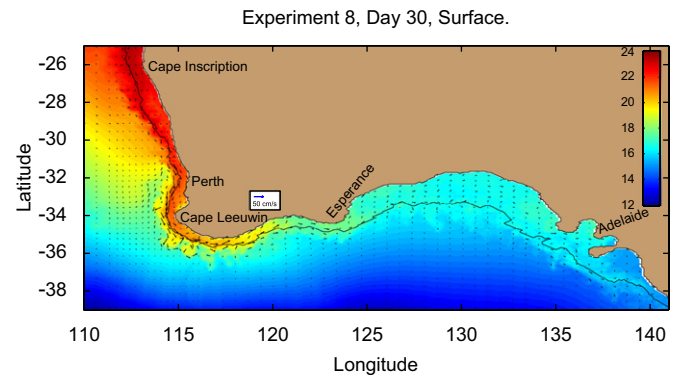**Fig. 11.** Experiment 8, day 30 sea surface temperature (°C) and velocity vectors.

eastward along the coast to ~17 cm s^{-1} at 125°E (not shown). An opposing westward undercurrent with more than one core lies beneath this coastal current which increases in strength as it flows westward from ~13 cm s^{-1} at 125°E (not shown) to ~19 cm s^{-1} at 117°E (not shown). There is also an eastward component to the shelf current over the entire Great Australian Bight (Fig. 11).

These results are similar to previous experiments using thermohaline forcing, which is expected since the Leeuwin Current has observed to be strongest in the fall and winter.

As a result, the addition of winter wind forcing has no noticeable impact.

5. Higher spatial resolution daily wind-forcing experiments

The daily wind-forcing experiments seek to isolate the effects of interannual and smaller-scale temporal variability on the current system. These model runs also use higher spatial resolution wind forcing than used in previous experiments to examine the effects of smaller-scale wind features on the current system. There is considerable interannual, seasonal, and smaller-scale variability in the winds along the southern coast of Australia which can lead to variability in the currents and sea surface temperature distribution (Ridgway and Condie, 2004; Herzfeld and Tomczak, 1997). These experiments, Experiments 9–11 (see Table 1) use daily wind forcing for winter 2001 (Experiment 9), summer 2001 (Experiment 10) and summer 2000 (Experiment 11). The higher spatial resolution of the NOGAPS daily wind forcing represents an increase in resolution from $2.5° \times 2.5°$ of the ECMWF data set to $1° \times 1°$ for the NOGAPS data set. The wind field structure is quite similar to the ECMWF wind field off the western coast of Australia where there is little variability in the direction of the wind, but along the southern coast and especially in the Great Australian Bight, the NOGAPS wind field provides greater detail in the wind structure. Note that in all experiments the same bottom topography (Fig. 2) and coastline from the previous experiments are used.

5.1. Winter 2001 daily NOGAPS wind-forcing experiments

This experiment, Experiment 9 (see Table 1) used daily winds for June 2001 through August 2001 to force the model. The model was started from rest on June 1, 2001, and the daily winds for June were used to spin up the model. The analysis period of the model run is days 30 through 60, when the July, 2001 winds are used to force the model. The WOA94 monthly temperature (Fig. 3c) and salinity (not shown)) for January were also used.

As Fig. 12a and b illustrate, the broad onshore flow at the northern end of the model domain along the western coast was deflected to the south to produce a relatively narrow and swift poleward coastal current, the Leeuwin Current along the continental shelf break. The current is stronger than the summer case of Experiments 10 and 11 (see below). As in previous experiments, the band of warm water was advected southward and around Cape Leeuwin to the southern coast. The current remained eastward across the entire Great Australian Bight continental shelf for the duration of the model run and no upwelling was produced. A meander develops off Cape Leeuwin and there are several wave-like features in the sea surface temperature structure between Cape Leeuwin and Esperance.

Even though it is winter, an inshore current is equatorward at day 30 (Fig. 12a) over the southern end of the west coast and some upwelling is present in the embayment just north of Cape Leeuwin. This shows that, although an intermittent process, upwelling can be observed off the west coast in the winter. Note that by day 60 (Fig. 12b), more consistent with winter conditions, the inshore current becomes poleward and there is no upwelling in the embayment north of Cape Leeuwin.

The current system which forms in this experiment is qualitatively correct. Current speeds are comparable to observed values, and the current and temperature feature structures are quite realistic. Throughout the model run, realistic mesoscale features such as meanders and eddies form along the west coast. With the less variable winter winds, the more benign features
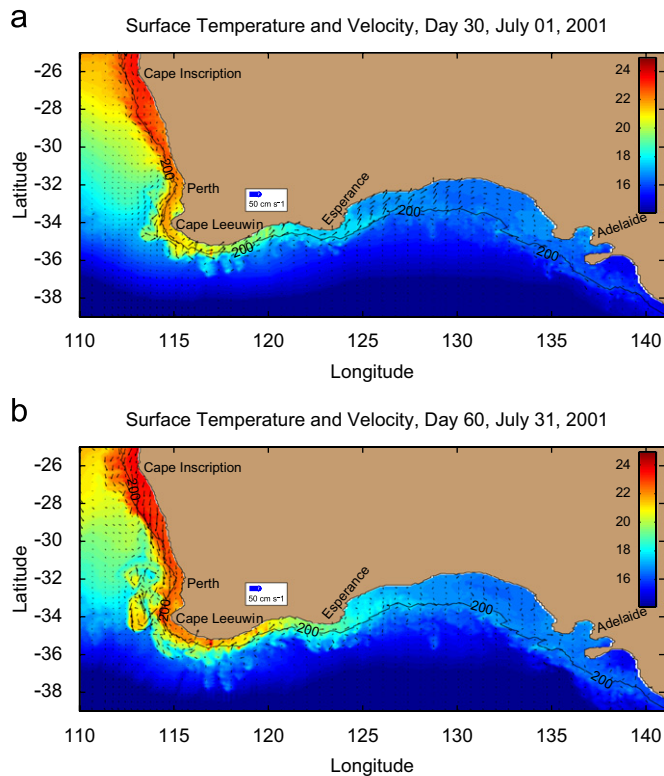
Fig. 12. Experiment 9 sea surface temperature (°C) and velocity vectors for (a) day 30, July 1, 2001 and (b) day 60, July 31, 2001.

along the southern coast were as expected with eastward flow and no upwelling in the Great Australian Bight.

Intermittently an equatorward flow and upwelling is present in the embayment just north of Cape Leeuwin. These features are consistent with the Capes Current, which is thought to be a summertime only current. This shows that, although an intermittent process, upwelling can be observed off the west coast in the winter, which is a new result.

5.2. Summer 2001 daily NOGAPS wind-forcing experiments

Experiment 10 (see Table 1) used daily winds for December 2000 through February 2001 to force the model. The model was started from rest on December 1, 2000, and the daily winds for December were used to spin up the model. The analysis period of the model run is days 30 through 60, when the January, 2001 winds are used to force the model. The WOA94 monthly temperature (Fig. 3b) and salinity (not shown) for January were also used.

As in previous experiments, the broad onshore flow at the northern end of the model domain along the western coast developed and was deflected to the south to produce a relatively narrow and swift poleward coastal current, the Leeuwin Current along the continental shelf break of the western coast (e.g., Fig. 13). The current was quite broad near its origin and it narrowed and increased in speed as it approached Cape Leeuwin. As in previous experiments, the band of warm water was advected southward then eastward as the current rounded Cape Leeuwin and flowed eastward along the southern coast. Intermittently, as Fig. 13 illustrates for day 45 (12 January, 2001), a relatively weak, inshore current flowed westward along the shore across much of the Great Australian Bight, but there was no convincing evidence of upwelling.
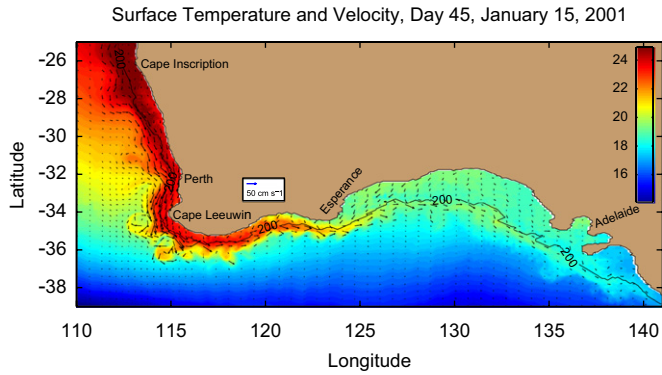
Surface Temperature and Velocity, Day 45, January 15, 2001

Fig. 13. Experiment 10 sea surface temperature (°C) and velocity vectors for January 2001.

5.3. Summer 2000 daily NOGAPS wind-forcing experiments

Since the westward current along the shore in the Great Australian Bight was only weak and intermittent and no upwelling developed during this model run, another summer daily wind model run was done for a different year. Experiment 11 (see Table 1) was run for December 1999 through February 2000. By day 30 (December 31, 1999), as shown in Fig. 14a, the westward current is already in place in the Great Australian Bight, with a thin ribbon of cooler upwelled water along the shore in the eastern end of the Bight. There is also cooler water at the surface at the western end of Kangaroo Island and south of Kangaroo Island between 138°E and 140°E. After day 30, the westward current over the Great Australian Bight shelf remains through day 39, then appears again at day 45 and again for days 57 through 60. Even though the current is reversing direction at day 42 (January 12, 2000; Fig. 14b), cooler water is visible at the surface along the eastern end of the Bight, along the western and northern shores of Kangaroo Island, and south of Kangaroo Island. Isotherms slope upward toward the shore in the eastern Great Australian Bight (not shown). South of Kangaroo Island, the upwelled pool is centered at ~37°N and the isotherms slope upward toward this pool from both the north and south (not shown). At day 60, the extent of upwelled water in the eastern Great Australian Bight is greater than before and the upwelled water remains in both locations near Kangaroo Island (not shown). As before, the isotherms slope upward toward the shore in the eastern Bight (not shown) and slope upward towards the cool surface water at 37°N from both directions (not shown).

The current system which formed in this summer daily wind model run was quite realistic. Mesoscale features formed along the west coast as expected (not shown). Even though the intermittent observed upwelling along the eastern Great Australian Bight and Kangaroo Island did not form in the 2001 model run (i.e., in Experiment 10), it did form when 2000 winds were used to force the model. This result is not unexpected, considering reports of significant interannual variability in the system (Ridgway and Condie, 2004).

5.4. Comparisons of model results with satellite SST imagery

Even though satellite SST imagery has not been able to resolve the exact structure of the circulation due to the complexity of the SST structure (Ridgway and Condie, 2004), it is useful to compare the model results with satellite imagery to form a qualitative assessment of model results. For this comparison, the model results are compared with multi-channel sea surface temperature (MCSST) satellite imagery provided by the Naval Oceanographic
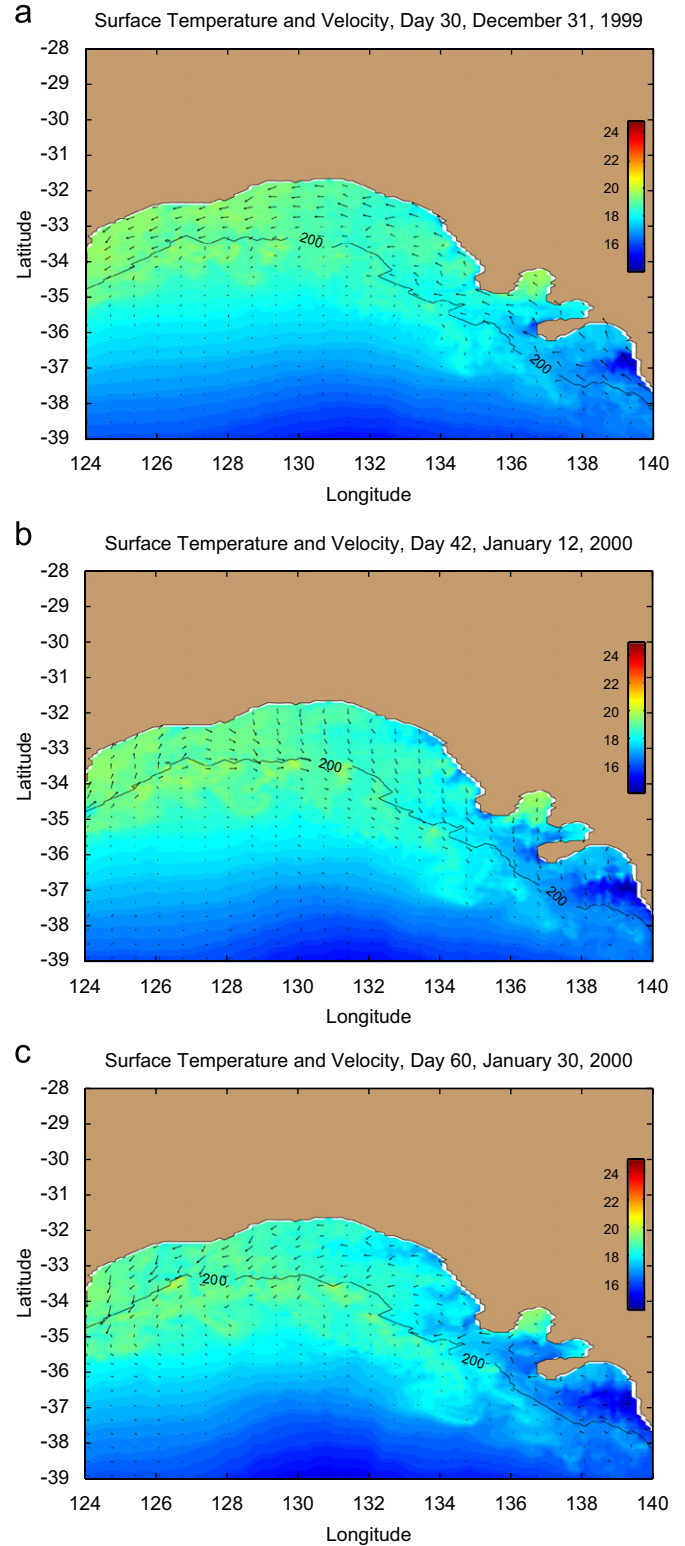
a Surface Temperature and Velocity, Day 30, December 31, 1999

b Surface Temperature and Velocity, Day 42, January 12, 2000

c Surface Temperature and Velocity, Day 60, January 30, 2000

Fig. 14. Experiment 11 sea surface temperature (°C) and velocity vectors in the Great Australian Bight (a) on day 30, December 31, 1999, (b) on day 42, January 12, 2000 and (c) on day 60, January 30, 2000.

Office (NAVO). MCSST temperatures are calculated by NAVO from the radiance values from the National Oceanic and Atmospheric Administration's (NOAA) polar orbiting advanced very high-resolution radiometer sensor (McClain et al., 1985). The imagery is a composite of data from the 7 days preceding the date of the

imagery. The original resolution of the AVHRR data is 4.4 km and the calculated MCSST temperatures are interpolated to a regular grid of 10 km resolution for presentation of the MCSST imagery.

The results of the winter Experiment 9 are compared to MCSST satellite imagery. In particular, the model run for day 60, July 31, 2001 (Fig. 12b) is compared against the MCSST imagery for July 31, 2001 (Fig. 15a). The location of the current along the west coast is similar. The satellite imagery shows an offshore bulge in the warm water near where the model develops an eddy north of Cape Leeuwin. The path of the current along the shelf break in the western Great Australian Bight is similar in the model and the imagery. The extent of warm water advection (~127°E) is approximately the same and the offshore features between 115°E and 120°E are present in both the model and the imagery.
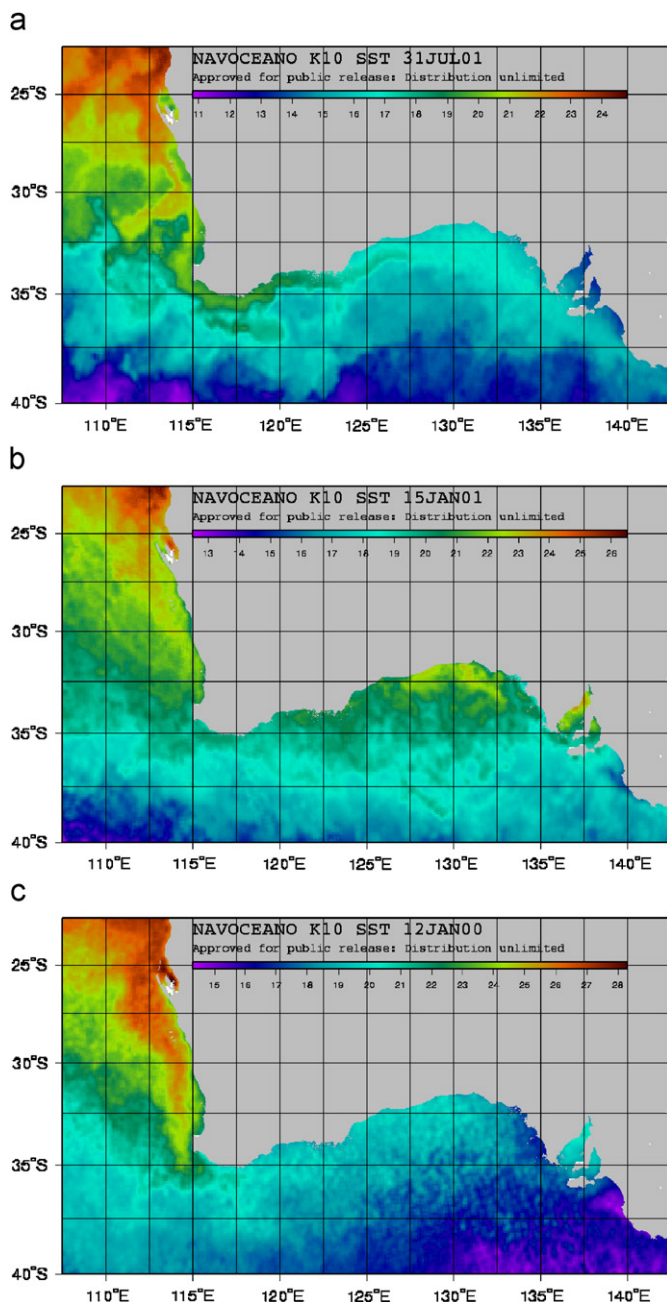

Fig. 15. Multi-channel sea surface temperature (MCSST) satellite imagery for southwestern Australia for (a) July 31, 2001, (b) January 12, 2000 and (c) January 15, 2001. Temperatures are in °C.

In the summer Experiment 10 modeled results for January 15, 2001 (Fig. 13), little if any, upwelling developed in the eastern Great Australian Bight. A very thin ribbon of slightly cooler water along the shore is visible in the MCSST imagery (Fig. 15b), consistent with very little upwelling. Farther east and south, both the model and the MCSST images show a cool pool south of Kangaroo Island.

In Experiment 11 (summer 2000), upwelling does develop and is similar to the satellite imagery both in intensity and location. At day 42, January 12, 2000 (Fig. 14b), the model upwelled ~16 °C water in the eastern Great Australian Bight. At the same time, the MCSST imagery (Fig. 15c) shows ~16.5 °C water in the same location, ~132.5°E to ~135.5°E. The Kangaroo Island pool is also similar to the imagery with modeled temperature of ~15 °C and satellite temperature of ~14.4 °C. Between these pools of cooler water, the Spencer Gulf is warmer with ~20 °C water in both the model results and satellite imagery. These results showing intermittent upwelling are also in agreement with recent CTD observations which show that the upwelling is intermittent (McClatchie et al., 2006b).

6. Summary remarks

This study was a numerical modeling study of the entire current system off western and southern Australia. While observations provide insight for the basic nature of features in the coastal current system, process-oriented studies are useful for systematically investigating the characteristics and dynamical forcing mechanisms for the currents and eddies in the current system. The results of these investigations should ultimately provide insight for interpreting observations and remotely sensed data in the region (e.g., Ridgway and Condie, 2004).

A series of process-oriented experiments, arranged in order of increasing complexity, sought to isolate which features in the current system are caused by which type of forcing (wind or thermohaline gradients) by applying each forcing individually and in various combinations, including with and without bottom topography. To isolate the effects of temporal variability, seasonal and then daily varying winds were added. To examine features generated by smaller-scale wind features higher spatial resolution wind forcing was also used with the daily varying winds. Here we provide a brief overview of highlights for all experiments.

The highlights of the annual wind forcing only experiments show that a continuous 5500 km coastal current system can be generated, even in the absence of topography. On the west coast, equatorward coastal currents in the direction of the wind and an opposing undercurrent are generated, the latter due to meridional variability in the wind stress and/or to the planetary beta effect. The addition of topography results in a stronger core of the surface current over the shelf break. This is due to the trapping effect of topographic beta, which prevents west coast currents from becoming broader and drifting offshore (the latter due to the planetary beta effect). On the southern coast, where planetary beta is not active, a broad and deep westward current trapped at the coast is generated, due to positive wind stress curl, which increases in strength from east to west. The addition of topography separates the westward surface flow into two separate cores, a weaker one at the coast and the other over the shelf break and continental slope, the latter location consistent with that of the Flinders Current. This shows that positive wind stress curl, which generates a westward current, and topography, which has a trapping effect over the shelf due to topographic beta, can play a combined role in generating features consistent with the Flinders Current.

The highlights of the annual thermohaline forcing only experiments also show that a continuous 5500 km coastal current system can be generated, even in the absence of topography. On the west coast, a coastal poleward current in the opposite direction of the wind and an opposing equatorward undercurrent can be generated, consistent with the Leeuwin Current and Leeuwin Undercurrent, respectively. On the southern coast, the eastward direction of the Leeuwin Current is indistinguishable from another surface current called the South Australian Current. A subsurface current consistent with some of the features of the Flinders Current (e.g., the increase in speed from east to west) is also generated due solely to thermohaline forcing, which is a new result. The decrease in speed of the subsurface flow from the southwest to the west coast is consistent with the Flinders Current providing source waters for the Leeuwin Undercurrent. The addition of topography traps the Leeuwin Current and/or Southern Australian Current over the shelf break, and the Leeuwin Undercurrent and the Flinders Current off the continental slope.

The highlights of the combined wind and thermohaline experiment show that, even in the absence of topography, a poleward (eastward) current and opposing undercurrent, due to the thermohaline forcing, can dominate at the coast; however, they would have reduced velocities on the west coast due to the wind forcing counteracting the thermohaline forcing to slow the current. With the addition of topography, the locations of features shift: Along the west coast there are regions of localized upwelling. At the shelf break there is a continuous 5500 km poleward (eastward) surface current, while off the continental slope there is a continuous equatorward (westward) under-current. Note that, off the southern coast, the strong core of the eastward surface flow due to the thermohaline forcing dominates over the shelf region so that the westward flow, that had been present as a surface current in the wind forcing only experiment, is present as a subsurface current. Offshore of the shelf break, there are meanders and eddies, which result from the opposition of surface and subsurface currents as well as from thermohaline and wind forcing.

The addition of topography shows that topography is responsible for the currents' shelf break locations. On the west coast, topographic beta due to the continental slope prevents currents from becoming broader and drifting offshore. The combination of wind forcing, thermohaline gradients and topography show that swift currents forced by thermohaline gradients are slowed to more realistic speeds by opposing wind and by topography. Meanders and eddies result from the opposition of surface and subsurface currents as well as from thermohaline and wind forcing. The results illustrate that the 5500 km long current system over the shelf break can be maintained year-long due to the two independent forcing mechanisms, their interactions, and the strong trapping effect of bottom topography.

The seasonal and daily wind-forcing experiments highlight both the seasonal and interannual variability of this complex current system. The Leeuwin Current along the western coast is slightly stronger in winter (July) than summer (January). There is much greater mesoscale activity in January when the opposing winds were strongest. The results also show that, although upwelling has been observed only in the summer in the Capes Current region, upwelling occurs intermittently in the 2001 winter but not in the 2001 summer. This illustrates that, depending on the strength of the forcing mechanism, such as strong equatorward winter 2001 winds, features such as upwelling on the west coast, usually thought to exist in the summer but only intermittently, can occur in different seasons. Along the southern coast, a gyre forms intermittently in the Great Australian Bight in summer, but the flow is constantly eastward across the entire shelf in winter. The production of upwelling in the Great Australian Bight during the 2000 summer but not during the 2001 summer is an indication of the importance of interannual variability. Overall, the results of this process-oriented study compare well with available observations off western and southern Australia.

Future studies should explore the role of remote forcing in El Nino and La Nina years for the entire 5500 km current system. How is the current system maintained when the Leeuwin Current is less intense, which is a feature known to occur during an El Nino? A range of numerical studies from process-oriented to forcing from general circulation models with paddlewheels (Middleton, 2006) along with the role of coastal trapped waves and the geographical set up of wind-forced flows (Suginohara, 1982; Leth and Middleton, 2004) will likely need to be implemented.

Acknowledgments

Appendix A.   Supplementary materials

The online version of this article contains additional supplementary data. Please visit doi:10.1016/j.csr.2008.11.011

References

Batteen, M.L., 1997. Wind-forced modeling studies of currents, meanders, and eddies in the California current system. Journal of Geophysical Research 102, 985–1010.

Batteen, M.L., Butler, C.L., 1998. Modeling studies of the Leeuwin current off western and southern Australia. Journal of Physical Oceanography 28 (11), 2199–2221.

Batteen, M.L., Huang, M.-J., 1998. The effect of salinity on density in the Leeuwin current system. Journal of Geophysical Research 103 (C11), 24,693–24,721.

Batteen, M.L., Rutherford, M.J., 1990. Modelling studies of eddies in the Leeuwin current: the role of thermal forcing. Journal of Physical Oceanography 20, 1484–1520.

Batteen, M.L., Haney, R.L., Tielking, T.A., Renaud, P.G., 1989. A numerical study of wind forcing of eddies and jets in the California current system. Journal of Marine Research 47 (3), 493–523.

Batteen, M.L., Rutherford, M.J., Bayler, E.J., 1992. A numerical study of wind and thermal forcing effects on the ocean circulation off western Australia. Journal of Physical Oceanography 22, 1406–1433.

Batteen, M.L., Cipriano, N.J., Monroe, J.T., 2003. A large-scale seasonal modeling study of the California current system. Journal of Oceanography 59, 545–562.

Batteen, M.L., Kennedy, R.A., Miller, H.A., 2007a. A process-oriented numerical study of currents, eddies and meanders in the Leeuwin current system. Deep-Sea Research II: Topical Studies in Oceanography 54 (8–10), 859–883.

Batteen, M.L., Martinho, A.S., Miller, H.A., McClean, J.L., 2007b. A process-oriented modelling study of the coastal Canary and Iberian Current system. Ocean Modelling 18, 1–36.

Blumberg, A.F., Mellor, G.L., 1987. A description of a three-dimensional coastal ocean circulation model. Three-Dimensional Coastal Ocean Models, Coastal Estuarine Sciences. 4: in: Heaps, N., (Ed.), AGU, Washington, D.C, pp. 1–16.

Chapman, D.C., 1985. Numerical treatment of cross-shelf open boundaries in a barotropic coastal ocean model. Journal of Physical Oceanography 25, 1060–1075.

Cirano, M., Middleton, J.F., 2004. Aspects of the mean wintertime circulation along Australia's southern shelves: numerical studies. Journal of Physical Oceanography 33 (3), 668–684.

Cresswell, G.R., Golding, T.J., 1980. Observations of a south-flowing current in the southeastern Indian Ocean. Deep-Sea Research 27, 449–466.

Deng, X., Hwang, C., Coleman, R., Featherstone, W.E., 2008. Seasonal and interannual variations of the Leeuwin current off Western Australia from TOPEX/Poseidon satellite altimetry. Terrestrial, Atmospheric and Oceanic Sciences 19 (1–2), 135–149.

Flather, R.A., 1976. A tidal model of the northwest European continental shelf. Memorial Society of Royal Sciences of Liege, Ser. 6 (10), 141–164.

Gersbach, G.H., Pattiartchi, C.B., Ivey, G.N., Cresswell, G.R., 1999. Upwelling on the south-west coast of Asutralia—source of the capes current? Continental Shelf Research 19, 363–400.

Gill, A.E., 1982. Atmosphere–Ocean Dynamics. Academic Press, Inc., Orlando, Florida, 662 pp.

Goerss, J.S., Phoebus, P.A., 1992. The Navy's operational atmospheric analysis. Weather and Forecasting 7, 232–249.

Godfrey, J.S., Ridgway, K.R., 1985. The large-scale environment of the poleward-flowing Leeuwin current, Western Australia: longshore steric height gradients, wind stresses and geostrophic flow. Journal of Physical Oceanography 15 (5), 481–495.

Godfrey, J.S., Vaudrey, D.J., Hahn, S.D., 1986. Observations of the shelf-edge current south of Australia, Winter 1982. Journal of Physical Oceanography 16 (4), 668–679.

Griffiths, R.W., Pierce, A.F., 1986. Instability and eddy pairs on the Leeuwin Current south of Australia. Deep-Sea Research 32 (12), 1511.

Herzfeld, M., Tomczak, M., 1997. Numerical modeling of sea surface temperature and circulation in the Great Australian Bight. Progress in Oceanography 39, 29–78.

Hopkins, A., 2006. Sensitivity of bottom topography on the dynamics and sound speed structure in the northern Canary Current system. Naval Postgraduate School M.S. thesis, Monterey, California, 107 pp.

Leth, O., Middleton, J.F., 2004. A mechanism for enhanced upwelling off central Chile: eddy advection. Journal of Geophysical Research, C12020, (1029/2003JC002129).

Levitus, S., Boyer, T.P., 1994. Vol. 4: Temperature, NOAA Atlas NESDI 4, 117 pp., US Department of Commerce, Washington, DC, World Ocean Atlas.

Levitus, S., Burgett, R., Boyer, T.P., 1994. Vol. 3: Salinity, NOAA Atlas NESDI 3, 99 pp., US Department of Commerce, Washington, D.C, World Ocean Atlas.

Marchesiello, P., McWilliams, J.C., Shchepetkin, A., 2001. Open boundary conditions for long-term integration of regional oceanic models. Ocean Modelling 3, 1–20.

Martinho, A.S., Batteen, M.L., 2006. On reducing the slope parameter in terrain-following numerical ocean models. Ocean Modelling 13, 166–175.

McClatchie, S., Middleton, J., Pattiaratchi, C., Curnte, D., Kendrick, G., 2006a. The Southwest marine region: Part I Ecosystems National Oceans Office, Department of Environment and Heritage, Commonwealth Government of Australia, 142 pp.

McClatchie, S., Middleton, J.F., Ward, T., 2006b. Water mass analysis and alongshore variation in upwelling in the eastern great Australian bight. Journal of Geophysical Research 111, CO8007.

McClain, E.P., Pichel, W.G., Walton, C.C., 1985. Comparative performance of AVHRR based multichannel sea surface temperatures. Journal of Geophysical Research 90, 11587–11601.

McCreary Jr., J.P., Shetye, S.R., Kundu, P.K., 1986. Thermohaline forcing of eastern boundary currents: with application to the circulation off the west coast of Australia. Journal of Marine Research 44, 71–92.

Mellor, G.L., 2004. User's guide for a three-dimensional, primitive equation, numerical ocean model, 56 pp, Program in Atmospheric and Ocean Sciences Report, Princeton University, Princeton, N. J.

Mellor, G.L., Yamada, T., 1982. Development of a turbulence closure model for geophysical fluid problems. Reviews of Geophysics and Space Physics 20, 851–875.

Mellor, G.L., Oey, L.-Y., Ezer, T., 1998. Sigma coordinate pressure gradient errors and the seamount problem. Journal of Atmospheric and Ocean Technology 15, 1122–1131.

Meuleners, M.J., Pattiaratchi, C.B., Ivey, G.N., 2007. Numerical modeling of the mean flow of the Leeuwin Current system. Deep-Sea Research part II: Topical Studies in Oceanography 54 (8–10), 837–858.

Meuleners, M.J., Ivey, G.N., Pattiaratchi, C.B., 2008. A numerical study of the eddying characteristics of the Leeuwin Current System. Deep-Sea Research Part I: Oceanographic Research Papers 55 (3), 261–276.

Middleton, J.F., 2006. The coastal trapped wave paddle as an open boundary condition. Ocean Modelling 12, 224–236.

Middleton, J.F., Bye, J.A.T., 2007. A review of the shelf-slope circulation along Australia's southern shelves: Cape Leeuwin to Portland. Progress in Oceanography 75 (1), 1–41.

Middleton, J.F., Cirano, M., 1999. Wind-forced downwelling slope currents: a numerical study. Journal of Physical Oceanography 29 (8), 1723–1743.

Middleton, J.F., Cirano, M., 2002. A northern boundary current along Australia's southern shelves: the flinders current. Journal of Geophysical Research 107 (C9) Article no. C03129.

Middleton, J.F., Leth, O., 2004. Wind-forced set-up of upwelling, geographical origins and numerical models: the role of bottom drag. Journal of Geophysical Research 109, C12019.

Middleton, J.F., Platov, G., 2003. The mean summertime circulation along Australia's southern shelves: A numerical study. Journal of Physical Oceanography 33 (11), 2270–2287.

Miller, H.A., 2006. Modeling studies of the coastal/littoral current system off Southern Australia. Naval Postgraduate School Ph.D. dissertation, Monterey, California, 400 pp.

Morrow, R., Fang, F., Fieux, M., Molcard, R., 2003. Anatomy of three warm-core Leeuwin Current eddies. Deep-Sea Research 50, 2229–2243.

Palma, E.D., Matano, R.P., 1998. On the implementation of passive open boundary conditions for a general circulation model: the barotropic mode. Journal of Geophysical Research 103 (C1), 1319–1341.

Palma, E.D., Matano, R.P., 2000. On the implementation of passive open boundary conditions for a general circulation model: the three-dimensional case. Journal of Geophysical Research 105 (C4), 8605–8627.

Pearce, A.F., Pattiaratchi, C.B., 1999. The capes current: a summer countercurrent flowing past Cape Leeuwin and Cape Naturaliste, Western Australia. Continental Shelf Research 19, 401–420.

Rennie, S.J., Pattiaratchi, C.B., McCauley, R.D., 2007. Eddy formation through the interaction between the Leeuwin current, Leeuwin undercurrent and topography. Deep-Sea Research Part II: Topical Studies in Oceanography 54 (8–10), 818–836.

Ridgway, K.R., Condie, S.A., 2004. The 5500-km-long boundary flow off western and southern Australia. Journal of Geophysical Research 109 (C4) Article. no. C04017.

Rochford, D.J., 1986. Seasonal changes in the distribution of Leeuwin current waters off southern Australia. Australian Journal of Marine and Freshwater Research 37 (1), 1–10.

Roed, L.P., Smedstad, O.M., 1984. Open boundary conditions for forced waves in a rotating fluid. SIAM Journal on Scientific and Statistical Computing 5, 414–426.

Schott, F.A., McCreary, J.P., 2001. The monsoon circulation of the Indian Ocean. Progress in Oceanography 51 (1), 1–123.

Smith, W.F., Sandwell, D.T., 1997. Global seafloor topography from satellite altimetry and soundings. Science 277, 1956–1962.

Smith, R.L., Huyer, A., Godfrey, J.S., Church, J.A., 1991. The Leeuwin current off Western Australia, 1986–1987. Journal of Physical Oceanography 21 (2), 323–345.

Suginohara, N., 1982. Coastal upwelling: onshore–offshore circulation, equatorward coastal jet and poleward undercurrent over a continental shelf-slope. Journal of Physical Oceanography 12, 272–284.

Thompson, R.O.R.Y., 1984. Observations of the Leeuwin current off Western Australia. Journal of Physical Oceanography 14 (3), 623–628.

Thompson, R.O.R.Y., 1987. Continental-shelf-scale model of the Leeuwin current. Journal of Marine Research 45, 813–827.

Trenberth, K.E., Large, W.G., Olsen, J.G., 1990. The mean annual cycle in global ocean wind stress. Journal of Physical Oceanography 20 (11), 1742–1760.

Weaver, A.J., Middleton, J.H., 1989. On the dynamics of the Leeuwin current. Journal of Physical Oceanography 19, 626–648.

Woo, M., Pattiartchi, C., 2008. Hydrography and water masses off the western Australian coast. Deep-Sea Research Part I: Oceanographic Research papers 55 (9), 1090–1104.

Woo, M., Pattiartchi, C., Schroeder, W., 2006. Dynamics of the Ningaloo current off point cloates, Western Australia. Marine and Freshwater Resaerch 57 (3), 291–301.